

Accepted Manuscript

Pyrrolizines: design, synthesis, anticancer evaluation and investigation of the potential mechanism of action

Ahmed M. Gouda, Ahmed H. Abdelazeem, Hany A. Omar, Ashraf N. Abdalla, Mohammed A.S. Abourehab, Hamed I. Ali

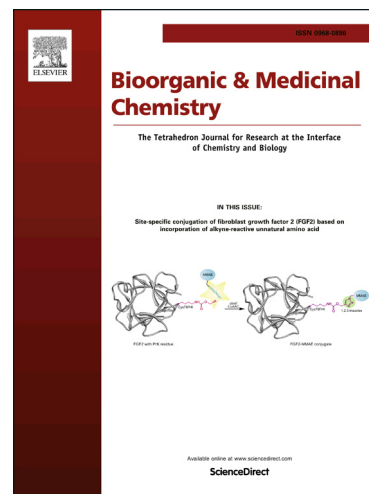
PII: S0968-0896(17)31494-3
DOI: <http://dx.doi.org/10.1016/j.bmc.2017.08.039>
Reference: BMC 13943

To appear in: *Bioorganic & Medicinal Chemistry*

Received Date: 21 July 2017
Revised Date: 18 August 2017
Accepted Date: 22 August 2017

Please cite this article as: Gouda, A.M., Abdelazeem, A.H., Omar, H.A., Abdalla, A.N., Abourehab, M.A.S., Ali, H.I., Pyrrolizines: design, synthesis, anticancer evaluation and investigation of the potential mechanism of action, *Bioorganic & Medicinal Chemistry* (2017), doi: <http://dx.doi.org/10.1016/j.bmc.2017.08.039>

This is a PDF file of an unedited manuscript that has been accepted for publication. As a service to our customers we are providing this early version of the manuscript. The manuscript will undergo copyediting, typesetting, and review of the resulting proof before it is published in its final form. Please note that during the production process errors may be discovered which could affect the content, and all legal disclaimers that apply to the journal pertain.



Pyrrolizines: design, synthesis, anticancer evaluation and investigation of the potential mechanism of action

**Ahmed M. Gouda^{1,2,*}, Ahmed H. Abdelazeem², Hany A. Omar^{3,4}, Ashraf N. Abdalla^{5,6},
Mohammed A.S. Abourehab⁷, Hamed I. Ali^{8,9,*}**

¹Department of Pharmaceutical Chemistry, Faculty of Pharmacy, Umm Al-Qura University, Makkah 21955, Saudi Arabia; ²Department of Medicinal Chemistry, Faculty of Pharmacy, Beni-Suef University, Beni-Suef 62514, Egypt; ³Sharjah Institute for Medical Research and College of Pharmacy, University of Sharjah, Sharjah 27272, United Arab Emirates; ⁴Department of Pharmacology and Toxicology, Faculty of Pharmacy, Beni-Suef University, Beni-Suef 62514, Egypt; ⁵Department of Pharmacology and Toxicology, Faculty of Pharmacy, Umm Al-Qura University, Makkah 21955, Saudi Arabia; ⁶Department of Pharmacology Medicinal and Aromatic Plants Research Institute, National Center for Research, Khartoum 2404, Sudan; ⁷Department of Pharmaceutics, Faculty of Pharmacy, Umm Al-Qura University, Makkah 21955, Saudi Arabia; ⁸Department of Pharmaceutical Chemistry, Faculty of Pharmacy, Helwan University, Cairo, Egypt; ⁹Rangel College of Pharmacy, Health Science Center, Texas A&M University, Kingsville, Texas 78363, United States.

*** To whom correspondence should be addressed**

Ahmed M. Gouda, Ph.D. Department of Medicinal Chemistry, Faculty of Pharmacy, Beni-Suef University, Beni-Suef 62514, Egypt.

Tel.: +2010-0287-7405

Fax: +2082-231-7958

E-mail address: ahmed.gouda@pharm.bsu.edu.eg, amsaid@uqu.edu.sa

Hamed I. Ali

Rangel College of Pharmacy, Health Science Center, Texas A&M University, Kingsville, Texas 78363, United States.

Tel.: +1361-221-0758

Fax: +1361-221-0793

E-mail address: alyismail@pharmacy.tamhsc.edu

List of abbreviations

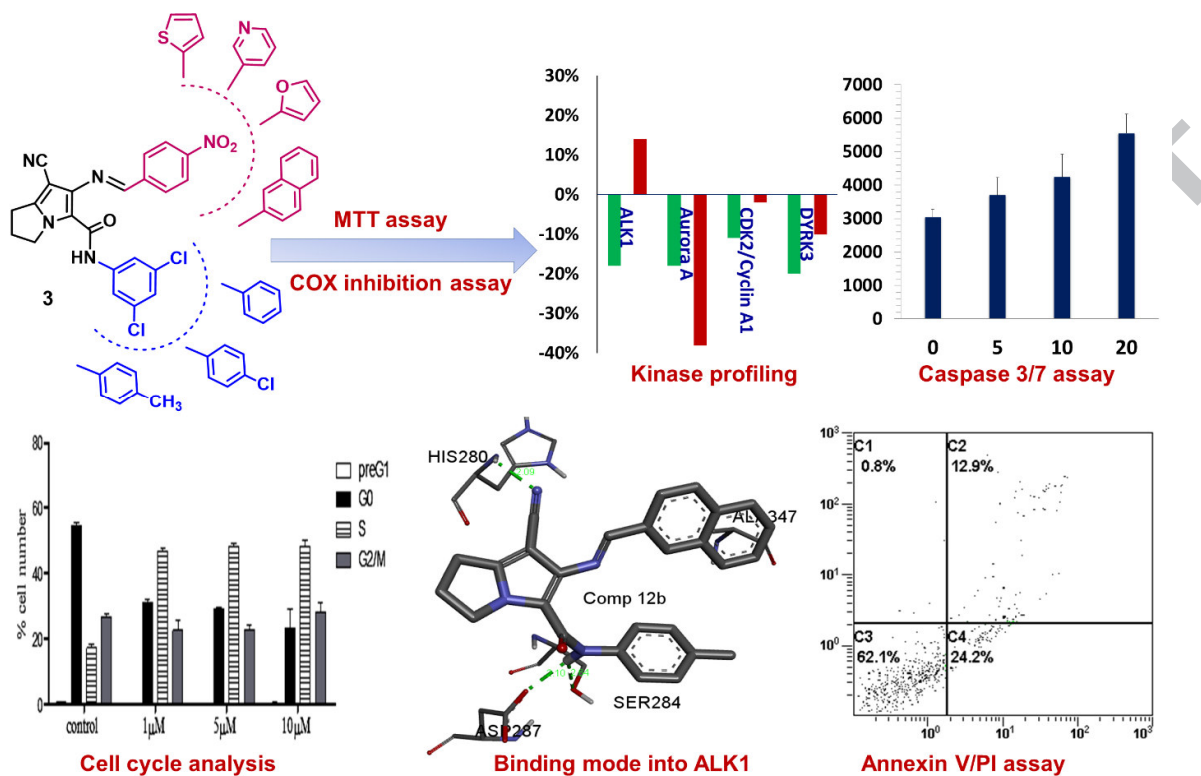
ALK1, activin receptor-like kinase; CDCl₃, deuterated chloroform; MTT, 3-(4,5-dimethylthiazol-2-yl)-2,5-diphenyl tetrazolium bromide; DSV, discovery studio visualizer; DYRK3, dual specificity tyrosine phosphorylation-regulated kinase; CDK2, cyclin-dependent kinase-2; COX, cyclooxygenase; DMSO, dimethyl sulfoxide, EGFR, epidermal growth factors receptor; eV, electron volte; FITC, fluorescein isothiocyanate; GSK3, glycogen synthase kinase-3; HEPES: 4-(2-hydroxyethyl)-1-piperazineethane- sulfonic acid; IC₅₀, half maximal inhibitory concentration; 5-LOX, 5-lipoxygenase; MAPK, mitogen-activated protein kinase; ODC, ornithine decarboxylase inhibitor; PBS, Phosphate-buffered saline; PC, pancreatic cancer; PDB, protein data bank; PI, propidium iodide; PPAR γ , peroxisome proliferator-activated receptor gamma; PS, phosphatidylserine; SAR, structure activity relationship; SEM, standard error of the mean; SI, selectivity index; VEGF, vascular endothelial growth factor.

Highlights

- A novel series of twelve pyrrolizines (**9-12a-c**) were designed and synthesized
- The anticancer activity was evaluated against MCF-7, A549, and Hep3B cells using MTT assay
- Compound **12b** showed IC₅₀ value of 3.24 μ M against A549 cell line
- The new compounds inhibited COX-1 and COX-2 with the selectivity index of 8.38-113.1 range
- Compound **12b** revealed a weak to moderate inhibition of six different protein kinases
- Compounds **12a** and **12b** exhibited the highest activation of caspase-3/7 in A549 cells
- Cell cycle analysis and Annexin V PI/FITC assay revealed an accumulation of MCF-7 tumor cells in the S-phase and an apoptotic induction by compound **12b**.

Key words. Pyrrolizine, anticancer, COX-2, Kinase, Caspase-3/7, Cell cycle, Annexin V, Apoptosis

Graphical Abstract



Abstract

A novel set of pyrrolizine-5-carboxamides has been synthesized and evaluated for their anticancer potential against human breast MCF-7, lung carcinoma A549 and hepatoma Hep3B cancer cell lines. Compound **10c** was the most active against MCF-7 with IC_{50} value of 4.72 μ M, while compound **12b** was the most active against A549 and Hep3B cell lines. Moreover, kinases/COXs inhibition and apoptosis induction were suggested as potential molecular mechanisms for the anticancer activity of the novel pyrrolizines based on their structural features. The new compounds significantly inhibited COX-1 and COX-2 with IC_{50} values in the ranges of 5.78-11.96 μ M and 0.1-0.78 μ M, respectively with high COX-2 selectivity over COX-1. Interestingly, the most potent compound in MTT assay, compound **12b**, exhibited high inhibitory activity against COX-2 with selectivity index (COX-1/COX-2) > 100. Meanwhile, compound **12b** displayed weak to moderate inhibition of six kinases with inhibition% (7-20%) compared to imatinib (inhibition% = 1-38%). The results of cell cycle analysis, annexin V PI/FITC apoptosis assay and caspase-3/7 assay revealed that compound **12b** has the ability to induce apoptosis. The docking results of compound **12b** into the active sites of COXs, ALK1 and Aurora A indicated that it fits nicely inside their active sites. Overall, the current study highlighted the significant anticancer activity of the newly synthesized pyrrolizines with a potential multi-targeted mechanism which could serve as a base for future studies and further structural optimization into potential anticancer agents.

1. Introduction

The persistent need for the development of new anticancer agents was augmented by several factors including the high rate of incidence and mortality of cancer, the poor bioavailability of some anticancer agents, and finally the evolution of resistance against many of the currently used anticancer agents [1-5].

As a multifactorial disease, treatment of cancer can be better achieved using multi-target therapy to overcome the resistance problem. Multi-target therapy can be obtained by either drug combination therapy or polypharmacology [6]. The combination of licoferone **1** (Fig. 1) with gefitinib exhibited significant reduction in pancreatic cancer (PC) at a dose lower than doses of the individual agents [7,8]. Moreover, combination of licoferone **1** with peroxisome proliferator-activated receptor gamma (PPAR γ) ligand and ornithine decarboxylase inhibitor (ODC) could provide chemopreventive and therapeutic effects [9-11]. Combination therapy showed an enhanced survival rate for the treatment of different types of cancers [12]. But, it still has some limitations, especially those related to the increased risk of drug-drug interaction and toxicity. On the other hand, anticancer agent with multi-targeted mechanism lack the problems of drug-drug interaction and dosage/sequences optimization needed in combination therapy.

The design of multi-targeted anticancer agents could provide an alternative approach for drug combination in complex diseases [13,14]. In anticancer research, several drugs act as multi-kinase inhibitors have displayed high therapeutic efficacy. But, another class of anticancer agents which can hit other targets together with or without kinase inhibition have been reported. Of these class, the dual COX/5-LOX inhibitor (licofelone) **1** has displayed potent anticancer activities against several types of hormonal dependent/independent cancer cells [15,16]. Exploring the mechanism of action of licoferone **1** revealed its ability to induce apoptosis [17].

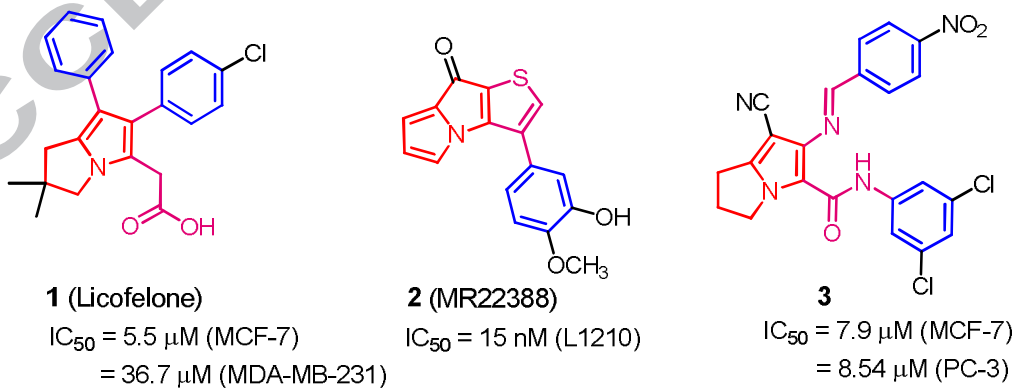


Fig. 1. Pyrrolizine-based anticancer agents with their IC_{50} values against different cancer cells

Tavolari *et al.* have presented a new evidence that the induction of apoptosis is mediated through mitochondrial pathway rather than COX inhibition and arachidonic acid pathway [18]. licofelone **1** displayed also indirect blockade of EGFR kinase, mitogen-activated protein kinase (MAPK) and AKT cascades. The inhibition of these kinases results from the changes in cell membrane fluidity and contribute at least in part to the induction of apoptosis in HCA-7 colon cancer cells [19].

Moreover, the tripentone (MR22388) **2** (**Fig. 1**) exhibited strong anticancer activity against leukemia L1210 cells with IC_{50} of 15 nM [20]. MR22388 induced apoptosis through the MAP kinase pathway and displayed strong inhibition of several other kinases, in addition to inhibition of tubulin polymerization [21-22].

We have previously reported compounds **3** among series of caspase-3/7 inducers [23]. Compound **3** displayed potent anticancer activity with IC_{50} values in the range of 7.9 and 8.54 μ M against MCF-7 and PC-3 cell lines respectively, **Fig. 1**.

Although the anti-inflammatory/anticancer potential of licofelone was extensively studied in several reports [24,25], but little data are available about its heteroaryl analogs. In the current work, we aimed to manipulate the chemical structure of the lead compound **3**. Based on the structure-activity relationship of licofelone [24]. We have designed the new analogs lacking the non-essential 3,3-dimethyl and carboxylic group, with 2 atoms spacer in between the pyrrolizine nucleus and phenyl rings, **Fig. 2**.

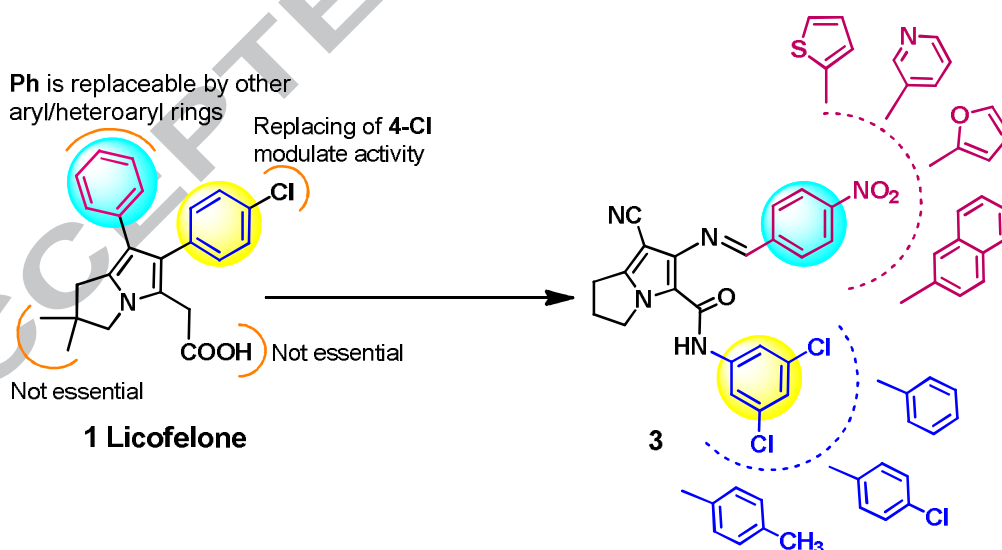


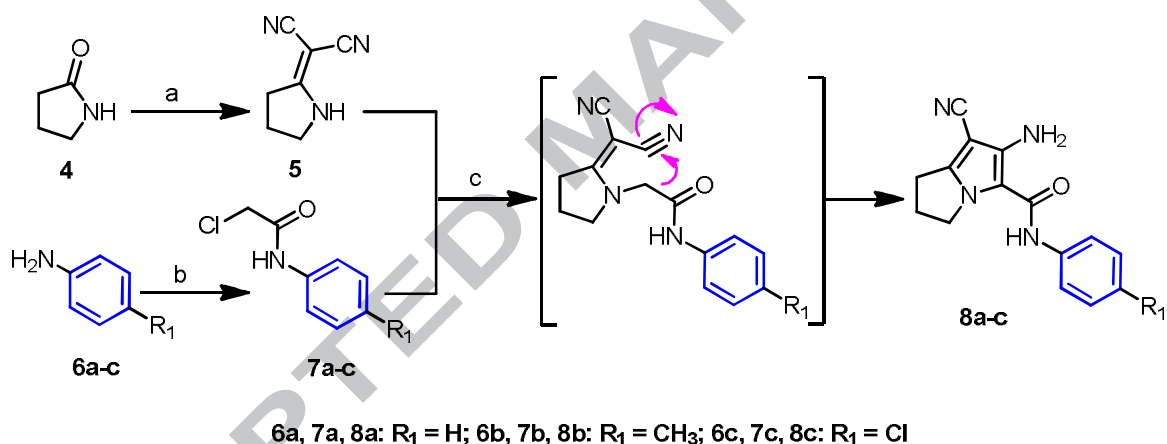
Fig. 2. Rational design and structural modification of compound 3

The new analogs were obtained through two modifications of the chemical structure of compound **3**, **Fig. 2**. The first was the replacement of the 4-nitrophenyl moiety by five-membered heterocyclic ring (furanyl or thiophenyl ring), six-membered (pyridinyl) ring or bulky (naphthalenyl) ring. The second modification was conducted through variation of the type of substituents on the second phenyl ring, using the 4-methyl (+ σ) and 4-chloro (- σ) substituents in addition to the unsubstituted analogs.

2. Results and discussion

2.1. Chemistry

Synthesis of compounds **5**, **7a-c** and **8a-c** (**Scheme 1**) was performed following the reported protocols [26-28].

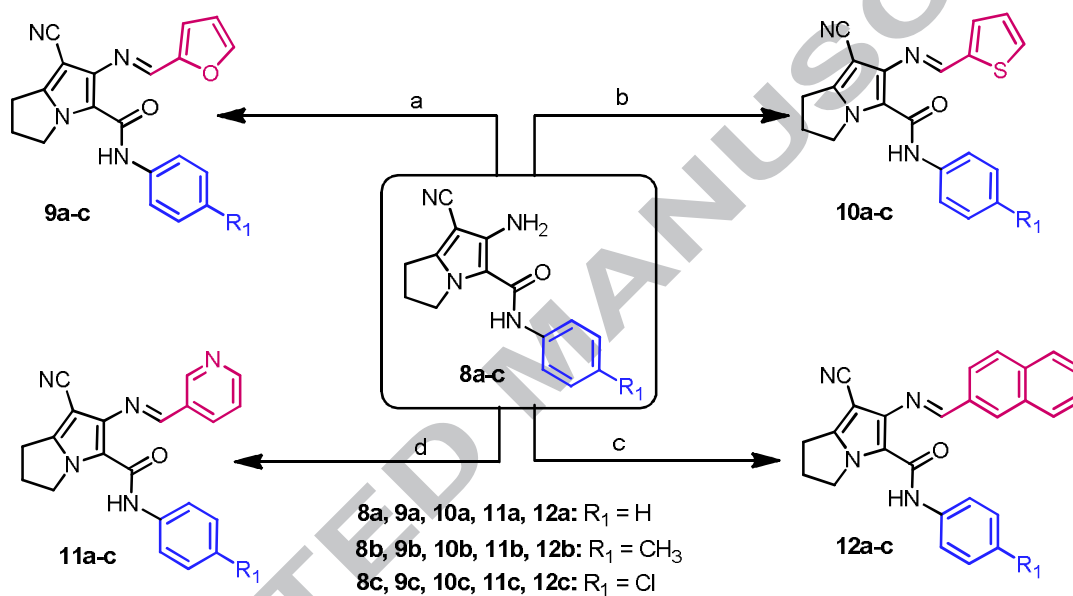


Scheme 1. Reagents and reaction conditions: (a) $(\text{CH}_3)_2\text{SO}_4$, benzene, $\text{CH}_2(\text{CN})_2$; (b) ClCH_2COCl , AcOH , CH_3COONa ; (c) K_2CO_3 , acetone, reflux, 24 h.

The Schiff's base derivatives **9-12** were prepared by refluxing the pyrrolizines **8a-c** with different aryl aldehydes including furan-2-carbaldehyde, thiophene-2-carbaldehyde, pyridine-3-carbaldehyde, or 2-naphthaldehyde in absolute ethanol in the presence of a catalytic amount of glacial acetic acid as depicted in **Scheme 2**.

The structural characterization of all the synthesized derivatives was accomplished using IR, $^1\text{H-NMR}$, $^{13}\text{C NMR}$, and mass spectroscopy, in addition to the elemental analyses. The IR spectra of compounds **9-12** revealed their characteristic absorption bands in the ranges of 3211-3421, 2204-2215, and 1656-1679 cm^{-1} corresponding to the amide, cyano, and carbonyl group,

respectively. The $^1\text{H-NMR}$ spectra of compounds **9-12** showed singlet signal owing to Ph-CH_3 protons assigned for compound **9b**, **10b**, **11b** and **12b** in a range of 2.34-2.36 ppm, a multiplet signal due to the protons of CH_2-2 at range of 2.48-2.62 ppm, triplet at the range of 2.90-3.12 ppm attributed to the CH_2-1 protons, another triplet at the range of 4.46-4.60 ppm corresponding to the CH_2-3 . The aromatic protons in compounds **9-12** appeared as a multiplet at the range of 6.62-9.17 ppm. The methylene protons (N=CH) in compounds **9-12** appeared as a singlet at the range of 88.8-9.97 ppm, while the amide protons (CONH) appeared as singlet at the range of 10.38-11.25 ppm.



Scheme 2. Reagent and reaction conditions: (a) pyridine-3-carbaldehyde, AcOH, EtOH, reflux, 4 h; (b) furan-2-carbaldehyde, AcOH, EtOH, reflux, 4 h; (c) thiophene-2-carbaldehyde, AcOH, EtOH, reflux, 4 h; (d) 2-naphthalaldehyde, AcOH, EtOH, reflux, 4 h.

The $^1\text{H-NMR}$ spectra of compounds **9a-c** revealed the aromatic protons of the 2-furanyl ring as a quartet signal attributed to the furanyl CH-4'' at the range of 6.62-6.64 ppm, the furanyl CH-3'' appeared as a doublet at the range of 6.99-7.03 ppm, while the furanyl CH-5'' appeared as a singlet at the range of 7.71-7.73 ppm. The $^1\text{H-NMR}$ spectra of compounds **10a-c** revealed the aromatic protons of the 2-thiophenyl ring as a triplet signal attributed to the furanyl CH-4'' at 7.17 ppm for compounds **10a,b**. The thiophene CH protons at positions 3'' and 5'' were detected as two doublets at the range of 7.49-6.61 ppm for compounds **10a,b**. The $^1\text{H-NMR}$ spectra of

compounds **11a-c** revealed the aromatic protons of the 3-pyridinyl ring as a triplet signal attributed to the pyridinyl CH-5" at 7.13 and 7.53 ppm for compounds **11a** and **11b**, respectively. The pyridinyl CH-4" and CH-6" appeared as two doublets at a range of 8.18-8.79 ppm, while the pyridinyl CH-2" appeared as singlet at a range of 9.15-9.17 ppm. The ^{13}C -NMR spectra of compounds **9-12** revealed signal at 20.86-24.57 ppm, corresponding to the aliphatic carbon of the methyl group in compounds **9b**, **10b**, **11b** and **12b**. The carbon signals of the three methylene groups of the pyrrolizine ring appeared in the range 24.38-50.27 ppm. The two signals at the range of 151.55-158.82 ppm are corresponding to the N=CH and C=O carbons. On the other hand, the mass spectra for compounds **9a-c-12a-c** revealed the molecular ion peaks at 344 (**9a**), 358 (**9b**), 378 (**9c**), 360 (**10a**), 374 (**10b**), 394 (**10c**), 355 (**11a**), 369 (**11b**), 389 (**11c**), 404 (**12a**), 418 (**12b**), and 438 (**12c**), respectively. The fragmentation patterns of these compounds were in concordance with their chemical structures.

2.2. Pharmacology

2.2.1. Anticancer activity

2.2.1.1. MTT assay results

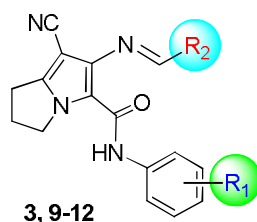
The growth inhibitory effect of the new compounds **9-12** against three cancer cell lines was performed to evaluate their anticancer activities. The target compounds were examined against MCF-7 (human breast cancer), A549 (lung carcinoma) and Hep3B (hepatoma) cell lines using MTT assay [29]. The results were expressed in IC_{50} and doxorubicin was used as a reference drug, **Table 1**. All the tested compounds showed inhibitory activities with IC_{50} values in the range of 3.24-34.75 μM against the three cancer cell lines. Compound **10c** was the most active against MCF-7 with IC_{50} value of 4.72 μM , while compound **12b** was the most active against both A549 and Hep3B cell lines.

2.2.1.2. Structure activity relationship (SAR)

Based on the MTT assay results, the structure activity relationship could be explained according to two main structural features; the steric bulkiness of the aryl/heteroaryl moiety in the side chain at C6 and the electronic effects of the various substituents on the phenyl ring. Correlating the results of the MTT assay (**Table 1**) with aryl/heteroaryl moiety bulkiness, it could be observed that the bulkiness of the aryl/heteroaryl ring has an important impact on the activity of the unsubstituted phenyl derivatives **9a**, **10a**, **11a** and **12a** where the electronic effect of methyl/chloro substituents was absent. Accordingly, the naphthalenyl derivatives **12a** was the most active compared to their corresponding thiophenyl and furanyl analogs. Conversely, the

three pyridinyl derivatives **11a-c** showed the least activity among all the new compounds against MCF-7 and Hep3G cell lines. Moreover, the thiophenyl bearing derivatives **10a-c** were nearly more active than their corresponding furanyl derivatives **9a-c** against the three cell lines.

Table 1. IC₅₀ values of compounds **9-12** against MCF-7, A549 and Hep3B cancer cell lines



Comp. No.	R ₁	R ₂	IC ₅₀ (μM)		
			MCF-7	A549	Hep3B
9a	H		8.35 ± 1.1	9.75 ± 1.2	12.80 ± 0.4
9b	4-CH ₃		16.15 ± 1.5	29.44 ± 2.4	24.41 ± 2.2
9c	4-Cl		15.68 ± 1.4	28.38 ± 3.4	27.52 ± 3.5
10a	H		6.97 ± 0.8	12.53 ± 2.6	18.62 ± 0.6
10b	4-CH ₃		5.35 ± 1.1	11.39 ± 1.6	13.75 ± 1.5
10c	4-Cl		4.72 ± 0.4	22.80 ± 1.3	11.62 ± 1.7
11a	H		11.65 ± 0.9	17.54 ± 3.2	25.82 ± 2.4
11b	4-CH ₃		18.26 ± 1.2	20.53 ± 1.9	34.75 ± 2.7
11c	4-Cl		22.52 ± 1.9	23.03 ± 1.3	31.17 ± 2.6
12a	H		5.77 ± 1.1	7.11 ± 0.7	10.17 ± 0.9
12b	4-CH ₃		7.76 ± 0.8	3.24 ± 0.3	8.69 ± 0.4
12c	4-Cl		9.82 ± 0.7	11.19 ± 0.8	12.49 ± 1.1
3	3,5-dichloro		7.9 ± 1.1 ^a	16.25 ± 1.5	14.04 ± 1.9
Licofelone	-	-	5.5 ± 0.6 ^b	-	-
Doxorubicin	-	-	2.3 ± 1.8	1.7 ± 1.1	2.4 ± 1.3

Cells were treated with the new compound or vehicle for 72 h. and the results were presented as mean ± S.E, ^a quoted from previous publication [23], ^b quoted from previous publication [16]

Concerning the impact of electronic effect of the 4-methyl/chloro substituents on activity of the new compounds, it was clear that, (1) The unsubstituted derivative **9a** was the most active in the three furanyl derivatives against both MCF-7 and A549 cell lines, followed by the chloro analog **9c** and finally the methyl analog **9b**. (2) The three thiophenyl derivatives **10a-c** displayed variable activity against the three cell lines where compound **10c** with the electron withdrawing chloro group was the most active against MCF-7 and Hep3B cells, while **10b** displayed the highest activity against A549 cell line. (3) Substitution with both electron donating methyl and electron withdrawing chloro groups reduced the activity of the pyridinyl derivatives where the unsubstituted analog **11a** displayed the highest activity against the three cell lines. (4) The 4-methyl substituent enhanced the anticancer activity of the naphthalenyl derivatives **12a-c** while the 4-chloro substitution decreased activity against both A549 and Hep3B cells.

2.2.2. *In vitro* COX-1/2 inhibitory activity

The discovery of several COX-2 selective inhibitors with potent anticancer activity represents an evidence for the important role of COX-2 receptor in regulation of cellular growth and death in human cancer [30-32]. In this work, COX-1/2 inhibition by the new compounds **9-12** was evaluated using COX colorimetric inhibitor screening assay kit (Catalog No. 560131, Cayman Chemicals INC., Ann Arbor, MI, USA). The assay was done following the manufacturer's instructions and as previously reported [33]. The results were expressed in IC₅₀ values, **Table 2**. The new compounds displayed inhibition of COX-1 and COX-2 with IC₅₀ values in the ranges of 5.78-11.96 μ M and 0.1-0.78 μ M respectively. Compound **11c** was the most active COX-1 inhibitor, while compound **11a** was the most active COX-2 inhibitor. The new compounds **9-12** displayed selective inhibition of COX-2 over COX-1 with selectivity index (SI) in the range of 8.38-113.1. Compound **11a** was the most selective for COX-2 (SI = 113.1) followed by compound **12b** (SI = 108.73), **Table 2**. A weak relationship was observed between the selectivity of the new compounds to COX-2 with their anticancer activity. Compound **12b**, the second selective COX-2 inhibitor in the new derivatives displayed the highest anticancer activity with IC₅₀ values in the range of 11.6-19.1 μ M against the three cell lines. The third selective COX-2 inhibitor (**10b**) displayed IC₅₀ values in the range of 16.9-28.9 μ M, being less active than **12b**. Moreover, lack of the anticancer activity of compound **11c** (IC₅₀ >60 μ M) was

associated with its very weak selectivity for COX-2 selectivity (SI = 8.5). Similarly, compounds **9c** and **10c** with selectivity index of 18.69 and 21.33 displayed $IC_{50} > 60 \mu M$ against MCF-7 cells.

Table 2: *In vitro* COX-1/2 enzymes inhibition results of compound **9-12**.

Comp. No	COX-1	COX-2	SI ^b
	(IC ₅₀ μM) ^a	(IC ₅₀ μM) ^a	
9a	6.54	0.78	8.38
9b	9.23	0.19	48.58
9c	8.41	0.45	18.69
10a	4.96	0.56	8.86
10b	10.41	0.11	94.64
10c	7.68	0.36	21.33
11a	11.31	0.10	113.10
11b	9.54	0.16	59.63
11c	5.78	0.68	8.50
12a	7.98	0.52	15.35
12b	11.96	0.11	108.73
12c	10.63	0.17	62.53
Indomethacin	0.039	0.49	0.0796
Celecoxib	14.8	0.05	296.0
Licofelone^a	0.21 ^b	4.7 ^b	0.045

^aIC₅₀ was calculated using three determinations for COX-1 (ovine) and COX-2 (human recombinant) screening assay kit (Cat. No 560131, Cayman Chemicals Inc., Ann Arbor, MI, USA); ^b*In vitro* COX-2 selectivity index (SI) = IC₅₀ of COX-1/ IC₅₀ of COX-2. ^b IC₅₀ values quoted from previous publication [24]

Taken together, a remarkable relationship between COX-2 selectivity of the new compounds and their anticancer activities could be observed. Compounds **10a-c** displayed higher selectivity against COX-2 enzyme than their furanyl analogs **9a-c** which was in agreement with the results of the MTT assay. Compound **12b** with the highest anticancer displayed high selectivity index of 108.73, **Table 2**. Compound **11a** with the highest selectivity for COX-2 showed potent activity against MCF-7 and moderate activity against A549 and Hep3G cell lines.

However, compounds **9a**, **10a** and **11c** which displayed different anticancer activities in MTT assay have nearly the same selectivity for COX-2. Moreover, compounds **10b** and **12c** which

displayed nearly the same anticancer activity against A549 cells displayed different selectivity for COX-2 enzyme. These findings suggested that COX-2 enzyme may not be the only target for the new compounds.

2.2.3. Kinase profiling radiometric assay

In attempt to explore other targets that may contribute to the mechanism of action of the new compounds as anticancer agents, the most active compound **12b** was selected for the kinase profiling test. The profiling test was done in KINEXUS Corporation, Vancouver, BC, Canada, using the radiolabeled ATP determination method. The test was done following the previous report [34]. The inhibitory activity of compound **12b** was evaluated against 20 kinases. The 20 kinases were selected from different groups, families and types including protein-tyrosine kinase and protein-serine/threonine kinase.

The results revealed that compound **12b** inhibits 6 kinases with inhibition% in the range of 7-20%, **Table 3**. Although this result showed weak to moderate inhibitory activity of compound **12b**, but it was higher than imatinib (inhibition% = 1-38). The highest inhibition caused by compound **12b** was against DYRK3 kinase (20%), followed by 18% inhibition in the enzyme activity of both ALK1 and Aurora A. Moreover, compound **12b** exhibited 11% inhibition in CDK2/Cyclin A1 kinase compared to only 2% for imatinib.

In conclusion, compound **12b** showed low to moderate inhibitory activity of 6 different kinases in comparison with imatinib. This finding suggests that kinase inhibition may participate partially to the overall anticancer activity of compound **12b**.

Table 3: The activation and inhibition of compound **12b** and imatinib against 20 different kinases at 10 μ M concentration.

Kinase	% Inhibition	
	12b	Imatinib
ALK1	-18%	14%
AMPK (A1/B1/G1)	11%	18%
ASK1	19%	5%
Aurora A	-18%	-38%
BLK	16%	-3%
BRAF	56%	13%
CDK2/Cyclin A1	-11%	-2%
CK1 Alpha 1	3%	0%
DYRK3	-20%	-10%
EGFR	47%	13%
EPHA1	37%	22%
FLT1	10%	-10%
GRK1	-7%	2%
GSK3 alpha	5%	-1%
MSK1	43%	49%
NEK1	-8%	-2%
p38 Alpha	28%	17%
PDK1	27%	34%
PRKG1	4%	4%
SGK1	16%	3%

Negative values indicate inhibition and positive value indicate activation

2.2.4. Caspase-3/7 activation assay

The role of caspase-3 and caspase-7 in as terminal enzymes in apoptosis was previously discussed [35,36]. Here in this study, it was of interest to evaluate the effect of the new compounds on these caspases using caspase 3/7 activation assay. Compounds **9a** and **12a-c**, the most active against lung carcinoma A549 cells were selected to evaluate their effect on caspase enzymes. Caspase 3/7 activity in A549 cells treated with compounds **9a** and **12a-c** was measured using caspase-Glo 3/7 luminescence assay kit (Promega, Madison, WI) following the manufacturer's instructions and as mentioned before [37]. Compounds **12a** and **12b** were the most potent in activating caspase enzymes in A549 cells at concentrations of 5, 10 and 20 μ M. In general, the results of caspase-3/3 activation assay were in concordance with the results of MTT assay in A549 cells, **Fig. 3**.

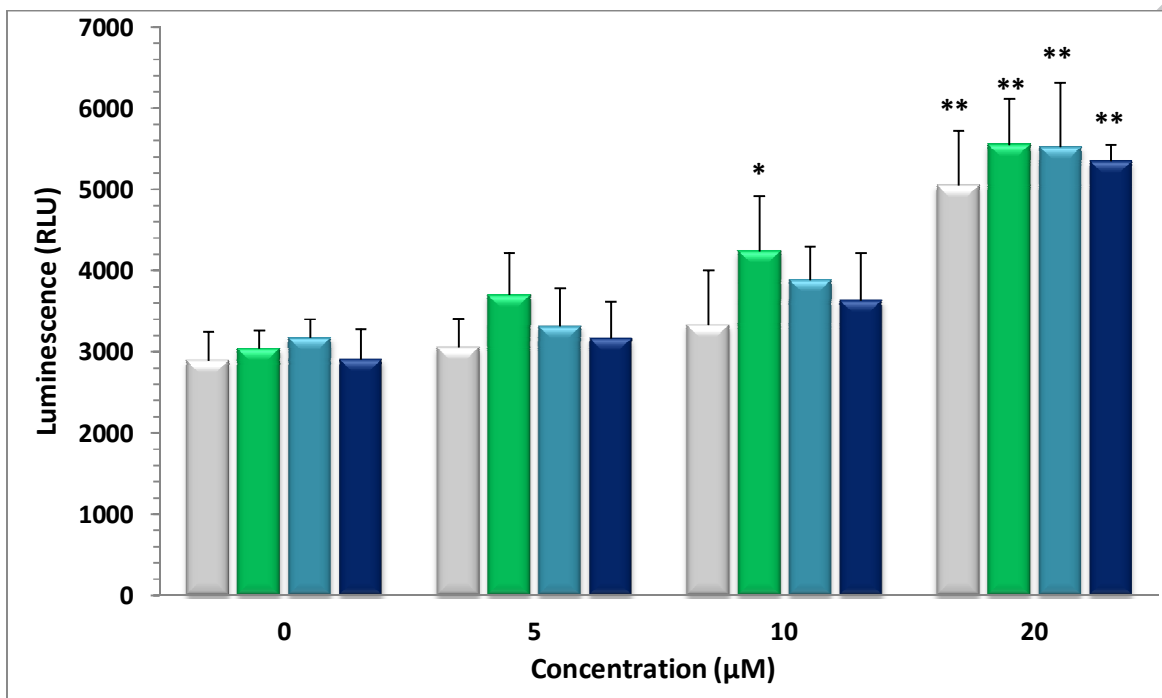


Fig. 3. Caspase-Glo 3/7 assay of lung carcinoma A549 cells treated with compounds **9a** (■), **12a** (■), **12b** (■), and **12c** (■) (24 h, x axis); luminescence (RLU, y axis). Experiment was repeated 3x. controls received equivalent amount of DMSO (vehicle). Columns, mean; bars, S.D. (n = 5). * p < 0.05, ** p < 0.01 as compared to vehicle (DMSO)-treated cells using one-way ANOVA followed by Dunnett's multiple comparison test

2.2.5. Determination of cell cycle perturbations

The cell division was analysed by flow cytometry using Propidium iodide-stained cell populations. The cell cycle analysis (BC, FC500) was conducted to test the effect of compound **12b** in MCF-7 cells (24 h) according to the reported protocol [38]. MCF-7 cells were treated by compound **12b** (1.0 μM), which demonstrated more than two-folds increase in S phase compared to control; this accumulation in S phase was maintained in the higher doses (5 and 10 μM); all at the expense of other stages, **Fig. 4**. Cells in G₂/M phase slightly increased at 10 μM, compared to control. The results indicate that compound **12b** caused considerable S phase arrest.

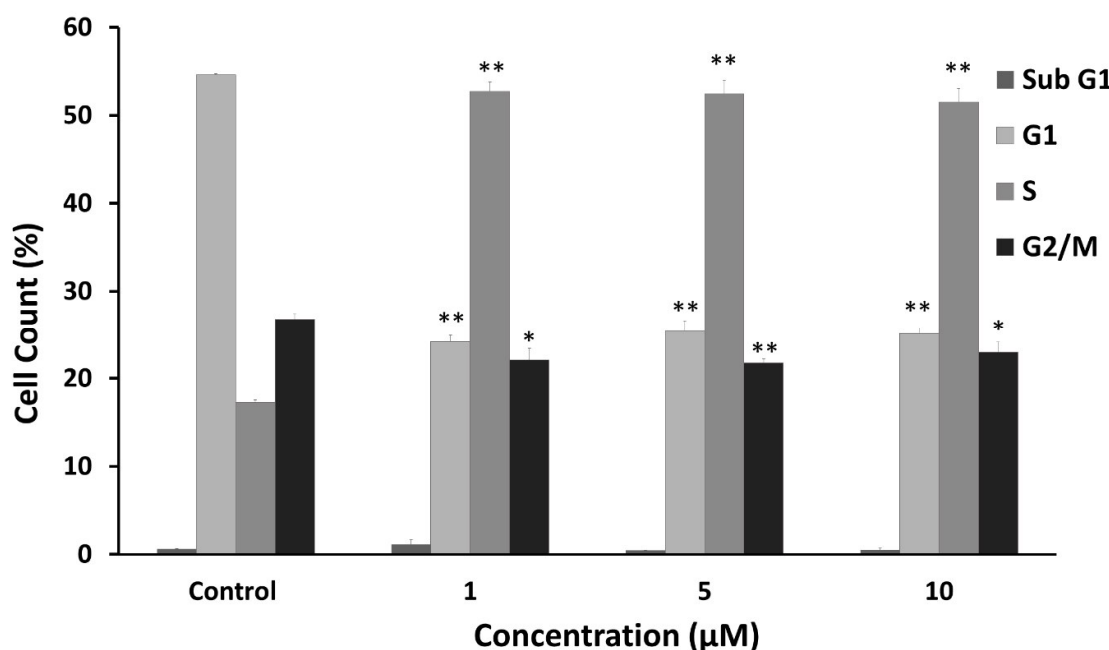


Fig. 4. Cell cycle phases of MCF-7 treated with compound **12b** for 24h (concentration, x axis); cell count (percent, y axis). Controls received equivalent amount of DMSO (vehicle). Columns, mean; bars, S.D. (n = 3). * p < 0.05, ** p < 0.01 as compared to vehicle (DMSO)-treated cells using one-way ANOVA followed by Dunnett's multiple comparison test

2.2.6. Annexin V PI/FITC apoptosis assay

Induction of apoptosis was reported to mediate the anticancer activity of licofelone [17]. Accordingly, compound **12b** the most active in MTT assay was selected for Annexin V apoptosis assay. MCF-7 cells were treated in this study with compound **12b** (24 h), then cells were double stained with Annexin PI/V FITC and analyzed by flow cytometry for detection of apoptosis according to the previous report [39]. The obtained results revealed MCF-7 cells in different phases according to their staining status. The results showed a slight increase in the apoptosis events (C2 and C4) at 1 µM compared to control, while in the higher doses cytotoxicity slightly increase, **Fig. 5**. At 1 µM, compound **12b** blocked MCF-7 in the S phase, which was consistent without increase in the higher doses; and increased apoptosis, suggesting that it is the therapeutic window.

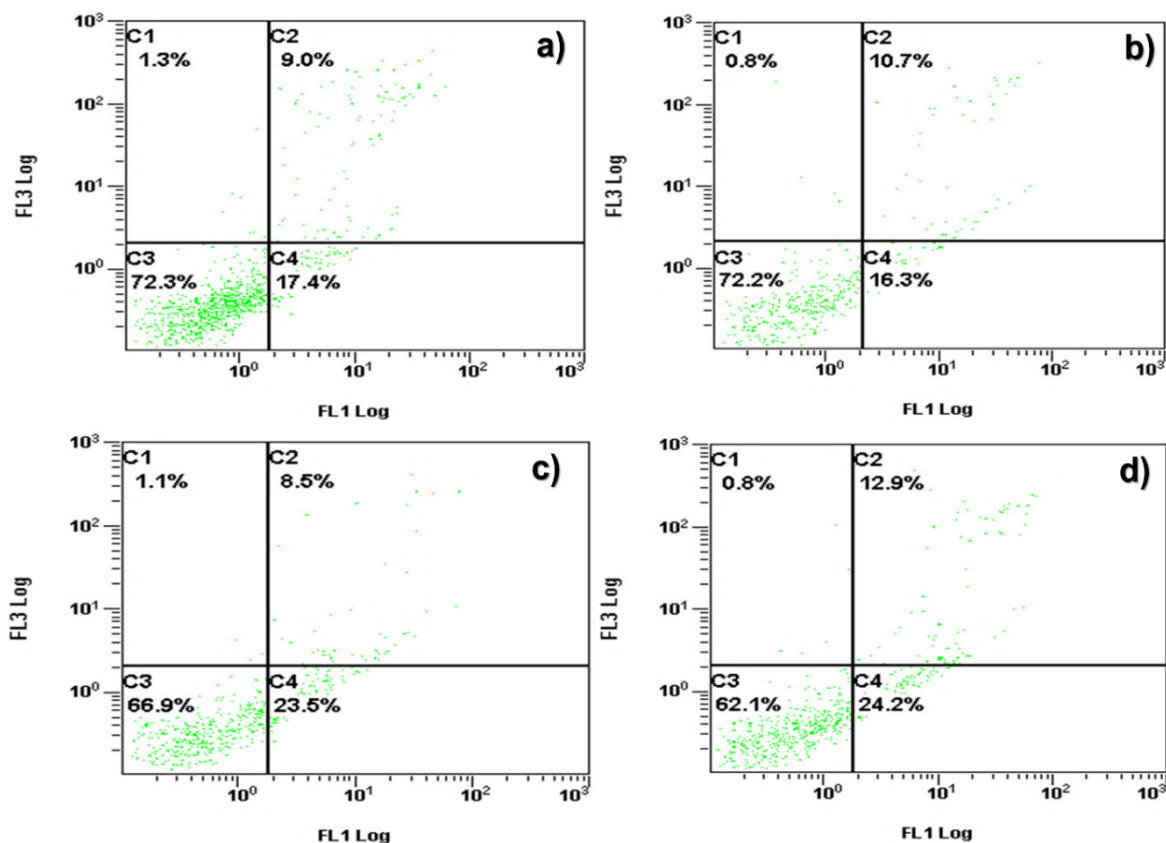


Fig. 5. Annexin V phases of MCF-7 cancer cells treated for 24 h with DMSO control (a), compound **12b** at 1 μ M (b), 5 μ M (c), 10 μ M (d); Data shown in the mean % \pm SD (n = 3). Experiment was repeated 3x.

2.3. Molecular docking study

The role of COX-2 receptor in cancers was supported by several evidences which described the anticancer potential of several COX-2 selective inhibitors [30-32]. Accordingly, the molecular docking study was conducted by comparative docking studies into COX-1/COX-2 and into the most targeted kinases namely: ALK1 and Aurora A kinases.

2.3.1. Comparative Docking study into COX-1 and COX-2 enzymes

GOLD 5.2.2. docking program was used for a differential docking study of compounds **9a-c**, **10a-c**, **11a-c**, and **12a-c** into COX-1 and COX-2 enzymes. The Gold score fitness, Gold score external vdw, and Gold score external hydrogen bonding (HB) are obtained as presented in

Table 1 for the best top five docked compounds. Our task for this docking study, is to compare the binding score fitness of each pose and to determine the best-fit docking style.

The Gold docking was initially validated by docking of the co-crystallized IBP ligand (ibuprofen) and RCX (vioxx) into COX-1 (PDB: 1eqg) and COX-2 (PDB: 5kir), respectively. Both of the docked ligands were almost superimposed on the co-crystallized one within a root mean square deviation (RMSD) of 0.64 and 0.81 Å, respectively as depicted in **Fig. 6**.

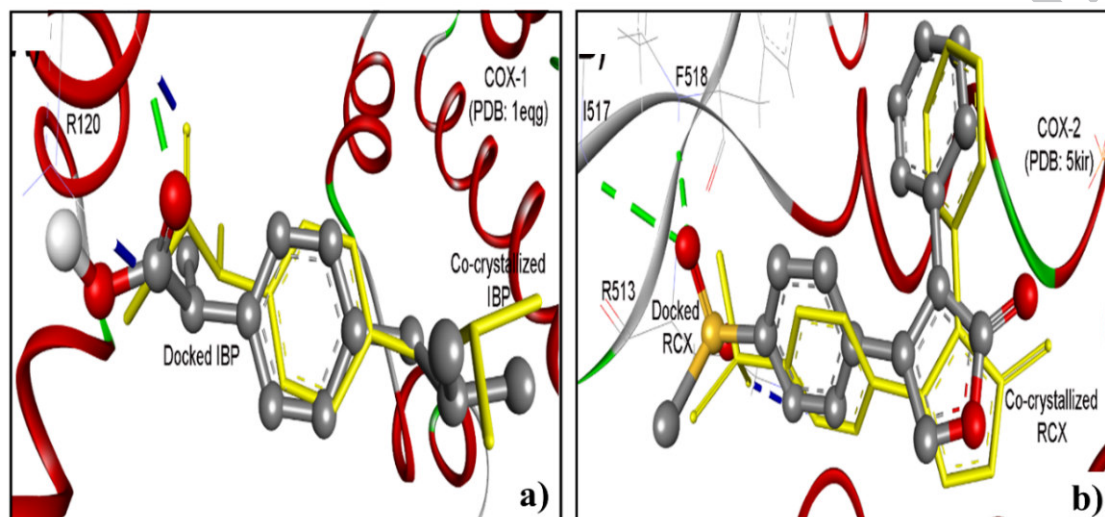


Fig. 6. a) Validation of the GOLD program by docking of ibuprofen into COX-1 (PDB: 1eqg); b) Validation of the GOLD program by docking of rofecoxib (Vioxx) into COX 2 (PDB: 5kir). The docked ligands (ball and stick) were identically superimposed on the co-crystallized IBP and RCX ligands (yellow sticks) within RMSD of 0.64 and 0.81 Å, respectively revealing a successful docking protocol.

Compounds **9a-c**, **10a-c**, **11a-c**, and **12a-c** were docked into COX-1 and COX-2 for a comparative binding study to correlate their differential selectivity with the experimental results. Remarkably, the docked compounds exhibited higher binding affinities into COX-2 of Goldscore fitness of the range of 73.73 -93.18. Whereas these compounds demonstrated inferior Goldscore fitness into COX-1 was with range of 28.78-62.23 as indicated in **Table 4**.

In addition, the assigned compounds were identically superimposed on the co-crystallized ligand (RCX601) in COX-2 enzyme of RMSD of 0.36-1.82 Å in a closer proximity than that of COX-1 (RMSD of 3.00-3.23 Å). These results distinctly demonstrated the higher selectivity of our compounds into COX-2 over COX-1.

Table 4. The docking results for the top five ranks of the compounds docked into COX-1 (1EQG) [40] and COX-2 (5KIR) [41] in comparison to the native bound inhibitors involving GOLD5.2.2

COX	Ligand	Gold Score Fitness	S (hb-ext) ^a	S (vdw-ext) ^b	Hydrogen bonds between compounds and COX enzymes		RMSD ^c (Å)
					Atom of compd.	Amino acid	
COX-1 ^e	9b	61.84	0.07	55.83		d	2.14
	9c	61.39	0.15	53.06	NHC=O	¹ HN of Arg120	3.00
					Furan-CH=N	¹ HN of Arg120	
	10a	62.23	0.86	52.90	NHC=O	² HN of Arg120	3.23
					Thiophen-CH=N	¹ HN of Arg120	
	10b	61.51	1.40	52.30	NHC=O	² HN of Arg120	3.02
					Thiophen-CH=N	¹ HN of Arg120	
10c	63.22	0.48	54.62	NHC=O	¹ HN of Arg120	3.06	
				Thiophen-CH=N	¹ HN of Arg120		
IBP701^f	51.13	9.58	71.08	<i>p</i> -C(CH ₃)C=O	¹ HN of Arg120	0.64	
COX-2 ^g	9b	85.11	1.73	56.35	Furan-O	¹ HN of Arg120	1.82
	9c	84.91	3.72	65.97		d	0.76
	12a	93.18	1.56	71.10	Ph-NHC=O	HO of Tyr355	0.39
	12b	88.15	1.65	68.13	Ph-NHC=O	HO of Tyr355	0.58
					7-CN	HN of Phe518	
	12c	88.21	1.82	69.44	Ph-NHC=O	HO of Tyr355	0.36
7-CN					HN of Phe518		
RCX601^h	72.23	2.89	51.82	<i>p</i> -S=O	HN of Ile517	0.81	
				<i>p</i> -S=O	HN of Phe518		

^a S(hb_ext) Gold score protein-ligand hydrogen bonding

^b S(vdw_ext): Gold score external Vdw (the van der waals interactions between protein and ligand)

^c RMSD: Root mean square deviation.

^d No hydrogen bond detected.

^e Ovine COX-1 complexed with ibuprofen

^f Ibuprofen: 2-(4-isobutylphenyl)propionic acid

^g Human COX-2 complexed with vioxx

^h Rofecoxib (Vioxx)

The docked compounds into COX-1 were bound into the binding site through up to four hydrogen bonds mainly with NH moiety of Arg120 amino acid. In addition, these compounds interacted hydrophobically revealing Gold score (external vdw) within a range of 34.91-55.83. In regard to COX-2, the designed compounds bound hydrophilically into the binding domain by up to two hydrogen bonds substantially with Tyr355 (OH), Phe518 (NH), and Arg120 (NH) and they docked deeply and robustly interacted hydrophobically by external vdw interactions within a range of 55.83-71.22. In this regard, compound **12b** exhibited remarkable Goldscore fitness of 88.15 into the binding domain COX-2 within 0.58Å from the native ligand (RCX) as shown in **Fig. 7**. It bound tightly into COX-2 by two hydrogen bonds with Tyr355 and Phe518 amino acids. Predominantly, compound **12b** interacts hydrophobically (vdw-ext: 69.44) into the binding site of COX-2 as shown in **Fig. 8**. Its naphthyl ring interacted by π -alkyl and π - π hydrophobic interactions with Leu352 and Trp387, respectively. Likewise, its *N*-(4-tolyl) moiety revealed π -alkyl interaction with Val349 and Ala527. And its 1*H*-pyrrolizine interacted by π -cation electrostatic interaction with Arg513 and hydrophobic-alkyl interaction with Ala516. The aforementioned results demonstrated that our designed and synthesized compounds namely **9b**, **9c**, and **12a-c** revealed a significant selectivity towards COX-2 over COX-1. Also, the calculated molecular docking results are correlated to a high extent to the experimental ones.

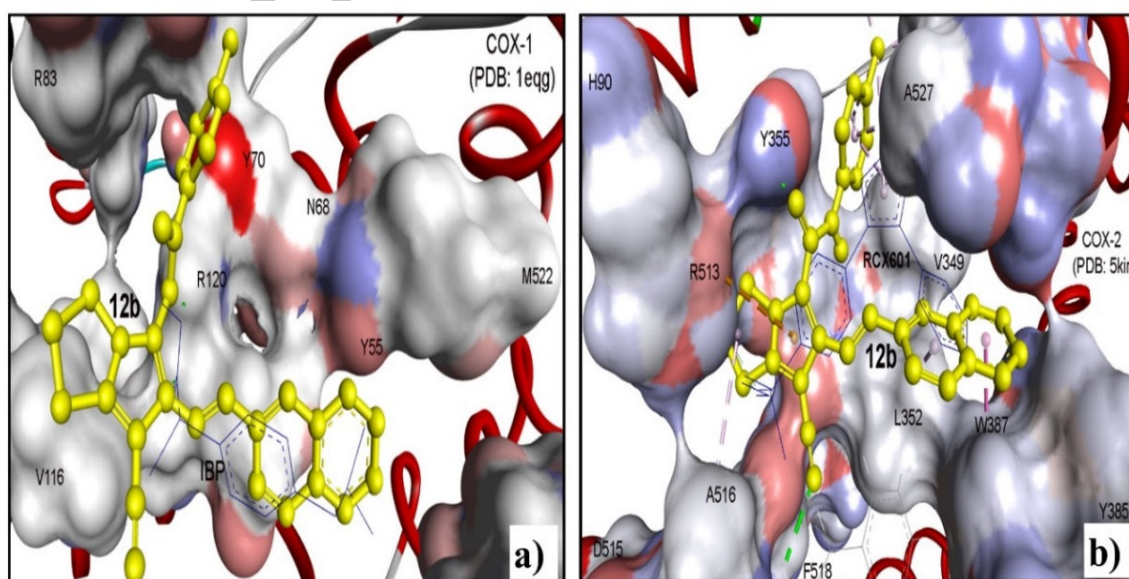


Fig. 7. a) Comparative docking mode of compound **12b** (yellow ball and stick) into COX1 (PDB: 1e9g), it exhibited a Goldscore fitness of 35.92, RMSD of 2.66Å, and one hydrogen bond with

Arg120; b) docking mode of compound **12b** into COX 2 (PDB: 5kir), it revealed a Goldscore fitness of 88.15, RMSD of 0.58Å, and two hydrogen bonds with Tyr355 and Phe518. (--) Hydrogen bond; (--) π -alkyl and π - π hydrophobic interaction; and (--) π -cation-electrostatic interaction.

2.3.2. Docking into ALK1 and Aurora A kinases

Targeting oncogenic such as ALK1, Aurora A, CDK2/cyclin A and DYRK3 represents important strategy in treatment of cancer and other diseases [42-46]. The docking results into ALK1 kinase (pdb code: 3MY0) [47] and Aurora A kinases (pdb code: 2W1C) [48] are presented in **Table 5** for compound **12b** in comparison to the co-crystallized ligands.

Compounds **12b**, the most active in MTT assay was selected to evaluate its inhibitory activity against 20 kinases. The results revealed that compound **12b** inhibited DYRK3A, ALK1, Aurora A and CDK2/cyclin A kinases with inhibition percent in the range of 11-20%. Although the inhibition of these kinases was apparently weak to moderate, but it was higher than that of imatinib. Docking studies were performed to investigate the binding modes and binding affinities of compound **12b** into the active site of ALK1 and Aurora A kinases. AutoDock 4.2 was used in these studies. The crystal structure of ALK1 (pdb code: 3MY0) [47] and Aurora A (pdb code: 2W1C) [48] were obtained from protein data bank (<http://www.rcsb.org/pdb>). The protein structure was prepared by delating water molecules and the native ligands. Validation of the docking studies were done by re-docking the native ligands with their corresponding kinases. The binding modes and interactions of the native ligands with the key amino acids in the active site were identified and compared with the reported data. The re-docked native ligands superimposed onto the position of the native ligands in the original pdb files.

Table 5. Results of the docking of compounds **12b** into ALK1 (pdb code: 3MY0) and Aurora A (pdb code: 2W1C) in comparison to the native ligands

Target Kinase	Ligand	ΔG_b^a (kcal/mol)	K_i^b	Atoms involved in H-bonding		Length ^d (Å)
				Ligand atom	Kinase moiety	
ALK1	12b	-10.58	17.48nM	N of CN	NH of HIS280	2.09
				O of CO	OH of SER284	2.64
				O of CO	OH of ASP287	2.10
	LDN	-10.33	26.98nM	NAT	NH of HIS280	2.37
				HAU1	O of ARG291	2.24
Aurora A	12b	-9.2	181.90nM	O of CONH	NH of ALA213	1.97
				N of CN	NH of THR217	2.62

			H34	O of ALA213	1.99
			N15	NH of ALA213	2.06
L0C	-8.94	281.04nM	H14	O of GLU211	2.20
			N24	O of PRO214	1.92 ^e

^a Binding free energy; ^b Inhibition constant; ^c Hydrogen bonds; ^d length in angstrom (Å),
^e electrostatic attraction (ionic bond).

The docking studies of compound **12b** into the active sites of ALK1 and Aurora A revealed a binding free energy (ΔG_b) of -10.58, -9.2, -10.83 and -10.54 kcal/mol, respectively. The binding modes of compound **12b** and the types of interactions with the amino acid in the active site of the three kinases were represented in **Fig. 8** and **Table 5**. Compound **12b** formed a network of hydrogen bonds within the active sites of ALK1 with HIS280, SER284 and ASP287 amino acids with bond length of 2.09, 2.64 and 2.10 Å, respectively.

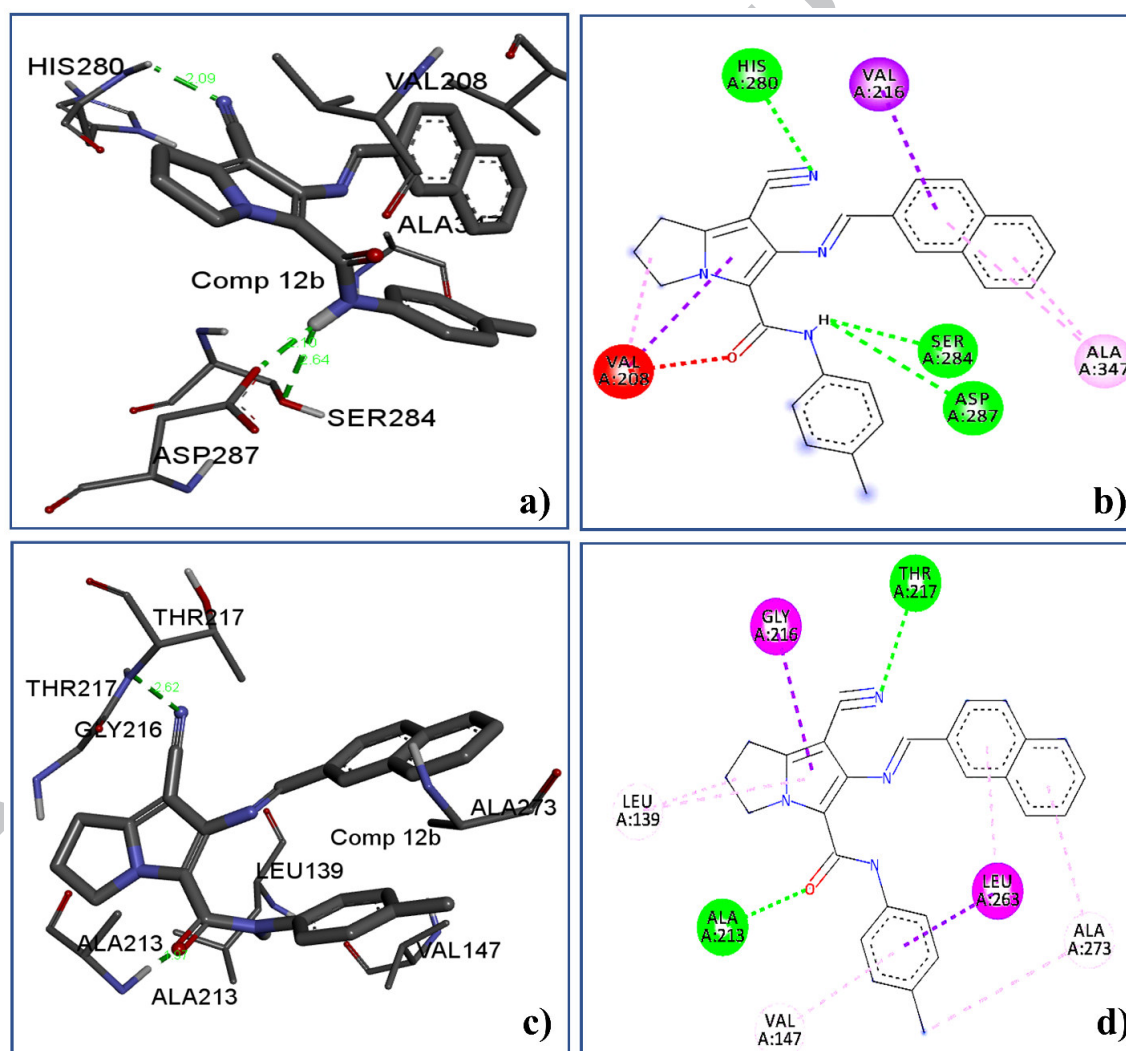


Fig. 8. a) 3D Docking mode of compound **12b** into ALK1 (pdb code: 3MY0); b) 2D Docking mode of compound **12b** into ALK1; c) 3D Docking mode of compound **12b** into Aurora A (pdb code: 2WIC); d)

2D Docking mode of compound **12b** into Aurora A. Hydrogen bonds were represented as (■ ■ ■), hydrophobic interactions including pi-sigma as (■ ■ ■), alkyl as (■ ■ ■) and pi-alkyl as (■ ■ ■) and unfavorable interaction as (■ ■ ■).

Moreover, five hydrophobic interactions of the pi-sigma, alkyl and pi-alkyl types were observed. Also, one unfavorable interaction between carbonyl oxygen in compound **12b** and VAL208 was formed. On the other hand, compound **12b** formed two hydrogen bonds with ALA213 and THR217 amino acids within the Aurora active site. In addition, seven hydrophobic interactions including pi-sigma, alkyl and pi-alkyl was observed.

3. Conclusion

In this study, a novel series of pyrrolizine-5-carboxamide has been synthesized and evaluated for their anticancer potential against a panel of human cancer cell lines. All the newly synthesized compounds showed IC₅₀ values in the range of 3.24-34.75 μM against the tested cell lines. Compound **10c** was the most active against MCF-7 with IC₅₀ value of 4.72 μM, while compound **12b** was the most active against A549 and Hep3B cell lines. Additionally, the new compounds displayed inhibition of COX-1 and COX-2 with IC₅₀ values in the ranges of 5.78-11.96 μM and 0.1-0.78 μM, respectively, being more selective for COX-2 over COX-1 with selectivity index (SI) in the range of 8.38-113.1. Compound **12b**, the most active compound in the MTT assay, was more than 100 time more selective for COX-2. The results of the kinase profiling revealed the ability of compound **12b** to inhibit various kinases with weak to moderate inhibition% in the range of 7-20% which is considered an appreciable activity in comparison with imatinib (inhibition% = 1-38%). The results of caspase activation assay revealed the ability of the new pyrrolizines to activate caspase-3/7 in A549 cells. Compounds **12a** and **12b** were the most potent in activating caspase enzymes in lung carcinoma A549 cells at 5, 10 and 20 μM. Cell cycle analysis and Annexin V PI/FITC apoptosis assay revealed that compound **12b** accumulated MCF-7 cells in the S phase and induced apoptosis. Docking studies of some selected compounds into the active site of COX-1/2, ALK1 and Aurora A were performed to study the binding pattern and binding free energy compared to the native ligands of these proteins. Totally, the activation of caspase-3/7, inhibitions of COX-2 and some kinases could contribute in part to the overall mechanism of action of the anticancer activity of the new compounds.

4. Experimental

4.1. Chemistry

All the chemical reagents and solvents used were purchased from Sigma-Aldrich. Solvents were dried according to the literature when necessary. The purity of the new compounds was checked with TLC using benzene-ethanol mixture (9:1). Melting points (m.p.) were determined by IA 9100MK-Digital melting point apparatus. Elemental analysis was performed at the microanalytical center, Cairo University. Infrared spectra (IR) were done using BRUKER TENSOR 37 spectrophotometer and expressed in wave number (cm^{-1}) using KBr disc (faculty of pharmacy, Umm Al-Qura University, KSA). The proton magnetic spectra were recorded on BRUKER APX400 spectrometer at 400 (faculty of pharmacy, Beni-Suef University, Egypt) and BRUKER AVANCE III at 500 MHz (faculty of pharmacy, Umm Al-Qura University, KSA) in chloroform and J constant are given in Hz. The ^{13}C -NMR spectra of the new compounds in chloroform were done at 100 and 125 MHz. Mass spectra were recorded using GCMS on Shimadzu Qp-2010 Plus mass spectrometer at 70 eV (EI) in the microanalytical center, Cairo University. Elemental analyses were done in the microanalytical center, Cairo University. Compounds **5**, **7a-c** and **8a-c** were prepared according to the previous reports [26-28].

4.1.1. General procedure for the preparation of compounds (9-12).

A mixture of pyrrolizine-5-carboxamides **8a-c** (2 mmol) and the aldehyde (2.2 mmol) in absolute ethanol (30 mL) in the presence of glacial acetic acid (0.5 ml) was refluxed for 4 hours. The reaction mixture was then concentrated, set aside to cool, whereby yellow crystals were formed, collected and recrystallized from chloroform-acetone (1:1).

4.1.1.1. (*EZ*)-7-Cyano-6-((furan-2-ylmethylene)amino)-*N*-phenyl-2,3-dihydro-1*H*-pyrrolizine-5-carboxamide (**9a**)

Compound **8a** was refluxed with furan-2-carbaldehyde to afford compound **9a** as yellow crystals, m.p. 227-30 °C, yield 75%. IR ν_{\max} /cm⁻¹ 3117 (NHs), 3049 (Ar C-H), 2215 (CN), 1673 (C=O). ¹H-NMR (CDCl₃-400 MHz) δ (ppm): 2.50 (m, 2H, pyrrolizine CH₂-2), 2.93 (t, 2H, *J* = 7.6 Hz, pyrrolizine CH₂-1), 4.49 (t, 2H, *J* = 7.3 Hz, pyrrolizine CH₂-3), 6.62 (q, 1H, *J* = 3.2 Hz, furanyl CH-4"), 6.99 (d, 1H, *J* = 3.4 Hz, furanyl CH-3"), 7.09 (t, 1H, *J* = 7.4 Hz, phenyl CH-4'), 7.35 (t, 2H, *J* = 7.8 Hz, phenyl CH-3'+CH-5'), 7.72 (s, 1H, furanyl CH-5"), 7.76 (d, 2H, *J* = 8.2 Hz, phenyl CH-2'+CH-6'), 8.88 (s, 1H, methylene amino (N=CH)), 11.13 (s, 1H, CONH). ¹³C-NMR (CDCl₃-100 MHz) δ (ppm): 24.38, 25.35, 50.01, 112.87, 116.32, 118.31, 118.60, 118.65, 119.35, 123.57, 128.97, 138.30, 138.81, 144.57, 146.62, 148.31, 151.55, 158.41. MS (EI): *m/z* (%) 346 (M⁺+2, 2), 345 (M⁺+1, 17), 344 (M⁺, 71), 343 (M⁺-1, 8), 327 (5), 316 (6), 299 (3), 252 (100), 224 (19), 196 (17), 184 (7), 169 (9) 156 (6), 141 (4), 106 (4), 95 (6), 80 (18). Anal. Calcd. for C₂₀H₁₆N₄O₂ (344.37): C, 69.76; H, 4.68; N, 16.27. Found: C, 69.95; H, 4.89; N, 16.72.

4.1.1.2. (EZ)-7-Cyano-6-((furan-2-ylmethylene)amino)-N-(4-tolyl)-2,3-dihydro-1H-pyrrolizine-5-carboxamide (**9b**)

Compound **8b** was refluxed with furan-2-carbaldehyde to afford compound **9b** as yellow crystals, m.p. 236-8°C, yield 78%. IR ν_{\max} /cm⁻¹ 3211 (NHs), 3050 (Ar C-H), 2214 (CN), 1673 (C=O), 1612 (C=C). ¹H-NMR (CDCl₃-400 MHz) δ (ppm): 2.34 (s, 3H, CH₃), 2.52 (m, 2H, pyrrolizine CH₂-2), 2.98 (t, 2H, *J* = 7.6 Hz, pyrrolizine CH₂-1), 4.51 (t, 2H, *J* = 7.3 Hz, pyrrolizine CH₂-3), 6.62 (q, 1H, *J* = 2 Hz, furanyl CH-4"), 7.01 (d, 1H, *J* = 3.4 Hz, furanyl CH-3"), 7.16 (d, 2H, *J* = 8.1 Hz, phenyl CH-3'+CH-5'), 7.65 (d, 2H, *J* = 8.2 Hz, phenyl CH-2'+CH-6'), 7.71 (s, 1H, furanyl CH-5"), 8.91 (s, 1H, methylene amino (N=CH)), 11.06 (s, 1H, CONH). ¹³C-NMR (CDCl₃-100 MHz) δ (ppm): 20.91 (CH₃), 24.44, 25.41, 50.02, 112.86, 116.37, 118.46, 118.52, 119.38, 119.41, 129.47, 133.14, 136.23, 138.21, 144.63, 146.55, 148.15, 151.69, 158.32. MS (EI): *m/z* (%) 360 (M⁺+2, 2), 359 (M⁺+1, 16), 358 (M⁺, 63), 357 (M⁺-1, 7), 341 (3), 330 (3), 291 (2), 252 (100), 224 (16), 196 (14), 184 (7), 169 (7), 156 (5), 141 (4), 129 (3), 106 (6), 95 (4), 80 (33). Anal. Calcd. for C₂₁H₁₈N₄O₂ (358.39): C, 70.38; H, 5.06; N, 15.63. Found: C, 70.78; H, 5.50; N, 15.45.

4.1.1.3. (EZ)-N-(4-Chlorophenyl)-7-cyano-6-((furan-2-ylmethylene)amino)-2,3-dihydro-1H-pyrrolizine-5-carboxamide (**9c**)

Compound **8c** was refluxed with furan-2-carbaldehyde to afford compound **9c** as yellow crystals, m.p. 260-2°C, yield 68%. IR ν_{\max} /cm⁻¹ 3272, 3223 (NHs), 2983 (Ar C-H), 2211 (CN), 1679

(C=O), 1618 (C=C). $^1\text{H-NMR}$ (CDCl_3 -400 MHz) δ (ppm): 2.55 (m, 2H, pyrrolizine CH_2 -2), 3.02 (t, 2H, $J = 7.6$ Hz, pyrrolizine CH_2 -1), 4.50 (t, 2H, $J = 8.0$ Hz, pyrrolizine CH_2 -3), 6.64 (q, 1H, $J = 3.5$ Hz, furanyl CH-4''), 7.03 (d, 1H, $J = 3.5$ Hz, furanyl CH-3''), 7.31 (d, 2H, $J = 8.8$ Hz, phenyl CH-3'+CH-5'), 7.72 (m, 3H, $J = 8.2$ Hz, phenyl CH-2'+CH-6' + furanyl CH-5''), 8.92 (s, 1H, methylene amino (N=CH)), 11.25 (s, 1H, CONH). $^{13}\text{C-NMR}$ (CDCl_3 -100 MHz) δ (ppm): 24.50, 25.42, 50.03, 113.01, 116.22, 118.15, 119.11, 120.48, 120.54, 128.38, 128.97, 137.42, 138.47, 144.69, 146.72, 148.41, 151.48, 158.44. MS (EI): m/z (%) 381 (M^++3 , 3), 380 (M^++2 , 13), 379 (M^++1 , 10), 378 (M^+ , 39), 377 (M^+-1 , 3), 350 (2), 326 (2), 310 (3), 283 (1), 252 (100), 224 (15), 196 (13), 184 (5), 169 (7), 156 (5), 141 (4), 129 (4), 106 (3), 95 (4), 80 (25). Anal. Calcd. for $\text{C}_{20}\text{H}_{15}\text{ClN}_4\text{O}_2$ (378.81): C, 63.41; H, 3.99; N, 14.79. Found: C, 63.83; H, 4.29; N, 14.43.

4.1.1.4. (EZ)-7-Cyano-N-phenyl-6-((thiophen-2-ylmethylene)amino)-2,3-dihydro-1H-pyrrolizine-5-carboxamide (10a)

Compound **8a** was refluxed with thiophene-2-carbaldehyde to afford compound **10a** as yellow crystals, m.p. 230-2 °C, yield 73%. $\text{IR}_{\text{vmax}}/\text{cm}^{-1}$ 3231 (NHs), 3086 (Ar C-H), 2212 (CN), 1667 (C=O). $^1\text{H-NMR}$ (CDCl_3 -500 MHz) δ (ppm): 2.49 (m, 2H, pyrrolizine CH_2 -2), 2.91 (t, 2H, $J = 7.5$ Hz, pyrrolizine CH_2 -1), 4.47 (t, 2H, $J = 7.1$ Hz, pyrrolizine CH_2 -3), 7.13 (t, 1H, $J = 7.3$ Hz phenyl CH-4'), 7.17 (t, 1H, $J = 4.0$ Hz, thiophenyl CH-4''), 7.38 (t, 2H, $J = 7.6$ Hz, phenyl CH-3'+CH-5'), 7.50 (d, 1H, $J = 3.0$ Hz, thiophenyl CH-3''), 7.61 (d, 1H, $J = 4.6$ Hz, thiophenyl CH-5''), 7.78 (d, 2H, $J = 8.0$ Hz, phenyl CH-2'+CH-6'), 9.23 (s, 1H, methylene amino (N=CH)), 10.48 (s, 1H, CONH). $^{13}\text{C-NMR}$ (CDCl_3 -125 MHz) δ (ppm): 24.40, 25.27, 50.20, 116.40, 117.76, 119.51, 119.59, 123.78, 128.61, 129.00, 131.48, 134.29, 138.42, 138.51, 141.92, 148.46, 151.80, 158.34. MS (EI): m/z (%) 363 (M^++3 , 1), 362 (M^++2 , 5), 361 (M^++1 , 16), 360 (M^+ , 62), 359 (M^+-1 , 7), 343 (3), 331 (4), 270 (6), 268 (100), 249 (4), 240 (13), 212 (9), 199 (3), 185 (7), 156 (6), 146 (2), 129 (3), 111 (9), 96 (6), 80 (25). Anal. Calcd. for $\text{C}_{20}\text{H}_{16}\text{N}_4\text{OS}$ (360.43): C, 66.65; H, 4.47; N, 15.54. Found: C, 66.48; H, 4.57; N, 15.11.

4.1.1.5. (EZ)-7-Cyano-6-((thiophen-2-ylmethylene)amino)-N-(4-tolyl)-2,3-dihydro-1H-pyrrolizine-5-carboxamide (10b)

Compound **8b** was refluxed with thiophene-2-carbaldehyde to afford compound **10b** as yellow crystals, m.p. 228-30 °C, yield 76%. $\text{IR}_{\text{vmax}}/\text{cm}^{-1}$ 3317, 3280 (NHs), 3076 (Ar C-H), 2212 (CN), 1656 (C=O), 1603 (C=C). $^1\text{H-NMR}$ (CDCl_3 -500 MHz) δ (ppm): 2.36 (s, 3H, CH_3),

2.48 (m, 2H, pyrrolizine CH₂-2), 2.90 (t, 2H, *J* = 7.6 Hz, pyrrolizine CH₂-1), 4.46 (t, 2H, *J* = 7.2 Hz, pyrrolizine CH₂-3), 7.17 (t, 3H, phenyl CH-3'+CH-5'+ thiophenyl CH-4''), 7.49 (d, 1H, *J* = 3.3 Hz, thiophenyl CH-3''), 7.60 (d, 1H, *J* = 4.8 Hz, thiophenyl CH-5''), 7.66 (d, 2H, *J* = 8.2 Hz, phenyl CH-2'+CH-6'), 9.22 (s, 1H, methylene amino (N=CH)), 10.41 (s, 1H, CONH). ¹³C-NMR (CDCl₃-125 MHz) δ (ppm): 20.94 (CH₃), 24.39, 25.28, 50.18, 116.44, 117.88, 119.46, 119.55, 128.58, 129.48, 131.42, 133.29, 134.18, 135.86, 138.30, 141.98, 148.34, 151.67, 158.20. MS (EI): *m/z* (%) 376 (M⁺+2, 2), 375 (M⁺+1, 6), 374 (M⁺, 22), 373 (M⁺-1, 2), 280 (48), 268 (37), 251 (3), 238 (8), 215 (9), 200 (2), 185 (2), 174 (9), 156 (2), 147 (70), 131 (4), 119 (100), 106 (52), 91 (33), 80 (36). Anal. Calcd. for C₂₁H₁₈N₄OS (374.46): C, 67.36; H, 4.85; N, 14.96. Found: C, 67.38, H, 4.89; N, 15.35.

4.1.1.6. (EZ)-N-(4-Chlorophenyl)-7-cyano-6-((thiophen-2-ylmethylene)amino)-2,3-dihydro-1H-pyrrolizine-5-carboxamide (10c)

Compound **8c** was refluxed with thiophene-2-carbaldehyde to afford compound **10c** as Yellow crystals, m.p. 250-2°C, yield 74%. IR_{v_{max}}/cm⁻¹ 3271, 3232 (NHs), 3003 (Ar C-H), 2204 (CN), 1666 (C=O). ¹H-NMR (CDCl₃-500 MHz) δ (ppm): 2.59 (m, 2H, pyrrolizine CH₂-2), 3.08 (t, 2H, *J* = 7.5 Hz, pyrrolizine CH₂-1), 4.55 (t, 2H, *J* = 7.1 Hz, pyrrolizine CH₂-3), 7.24 (broad s, 1H, thiophenyl CH-4''), 7.35 (d, 2H, *J* = 8.4 Hz, phenyl CH-3'+CH-5'), 7.65 (m, 2H, thiophenyl CH-3''+CH-5''), 7.77 (d, 2H, *J* = 8.4 Hz, phenyl CH-2'+CH-6'), 9.34 (s, 1H, methylene amino (N=CH)), 10.59 (s, 1H, CONH). ¹³C-NMR (CDCl₃-125 MHz) δ (ppm): 24.57, 25.42, 50.20, 116.20, 117.64, 120.94, 128.72, 128.76, 129.02, 131.47, 134.47, 137.02, 138.93, 141.97, 148.39, 152.24, 156.95, 158.47. MS (EI): *m/z* (%) 398 (M⁺+4, 2), 397 (M⁺+3, 6), 396 (M⁺+2, 20), 395 (M⁺+1, 17), 394 (M⁺, 50), 393 (M⁺-1, 10), 377 (1), 311 (1), 300 (2), 283 (2), 268 (100), 240 (11), 212 (6), 199 (2), 184 (6), 174 (6), 156 (5), 146 (3), 129 (4), 127 (5), 111 (6), 96 (3), 80 (36). Anal. Calcd. for C₂₀H₁₅ClN₄OS (394.88): C, 60.83; H, 3.83; N, 14.19. Found: C, 60.46; H, 4.24; N, 14.16.

4.1.1.7. (EZ)-7-Cyano-N-phenyl-6-((pyridin-3-ylmethylene)amino)-2,3-dihydro-1H-pyrrolizine-5-carboxamide (11a)

Compound **8a** was refluxed with pyridine-3-carbaldehyde to afford compound **11a** as yellow crystalline product, m.p. 233-4°C, yield 83%. IR_{v_{max}}/cm⁻¹ 3272, 3236 (NHs), 3012, 2922 (Ar C-H), 2215 (CN), 1667 (CO). ¹H-NMR (CDCl₃-400 MHz) δ (ppm): 2.58 (m, 2H, pyrrolizine CH₂-2), 3.07 (t, 2H, *J* = 7.6 Hz, pyrrolizine CH₂-1), 4.56 (t, 2H, *J* = 7.3 Hz, pyrrolizine CH₂-3), 7.13 (t, 1H, *J* = 7.4 Hz, pyridinyl CH-5''), 7.37 (t, 2H, *J* = 7.8 Hz, phenyl CH-3'+CH-5'),

7.49 (dd, 1H, $J = 7.7, 4.8$ Hz, phenyl CH-4'), 7.64 (d, 2H, $J = 7.8$ Hz, phenyl CH-2'+CH-6'), 8.22 (d, 1H, $J = 7.8$ Hz, pyridinyl CH-4''), 8.78 (d, 1H, $J = 7.4$ Hz, pyridinyl CH-6''), 9.17 (s, 1H, pyridinyl CH-2''), 9.23 (s, 1H, methylene amino (N=CH)), 10.46 (s, 1H, CONH). ^{13}C -NMR (CDCl_3 -100 MHz) δ (ppm): 24.56, 25.46, 50.27, 116.11, 118.46, 119.70, 122.12, 124.05, 124.22, 129.24, 131.13, 135.14, 138.03, 138.46, 148.49, 150.17, 152.74, 156.84, 158.23. MS (EI): m/z (%) 356 (M^++1 , 2), 355 (M^+ , 7), 277 (12), 263 (16), 236 (4), 207 (2), 194 (1), 180 (2), 153 (1), 127 (1), 117 (2), 106 (2), 91 (3), 80 (100). Anal. Calcd. for $\text{C}_{21}\text{H}_{17}\text{N}_5\text{O}$ (355.39): C, 70.97; H, 4.82; N, 19.71. Found: C, 71.17; H, 5.29; N, 20.16.

4.1.1.8. (EZ)-7-Cyano-6-((pyridin-3-ylmethylene)amino)-N-(4-tolyl)-2,3-dihydro-1H-pyrrolizine-5-carboxamide (11b)

Compound **8b** was refluxed with pyridine-3-carbaldehyde to afford compound **11b** as yellow crystalline product, m.p. 242-5°C, yield 87%. $\text{IR}_{\text{vmax}}/\text{cm}^{-1}$ 3279, 3178 (NHs), 3031, 2992 (Ar C-H), 2212 (CN), 1658 (C=O), 1597, 1568 (C=C). ^1H -NMR (CDCl_3 -500 MHz) δ (ppm): 2.35 (s, 3H, CH_3), 2.58 (m, 2H, pyrrolizine CH_2 -2), 3.06 (t, 2H, $J = 7.6$ Hz, pyrrolizine CH_2 -1), 4.56 (t, 2H, $J = 7.3$ Hz, pyrrolizine CH_2 -3), 7.19 (d, 2H, $J = 8.1$ Hz, phenyl CH-3'+CH-5'), 7.53 (t, 3H, phenyl CH-2'+CH-6'+pyridinyl CH-5''), 8.24 (d, 1H, $J = 7.9$, pyridinyl CH-4''), 8.79 (d, 1H, $J = 4.4$, pyridinyl CH-6''), 9.15 (s, 1H, pyridinyl CH-2''), 9.23 (s, 1H, methylene amino (N=CH)), 10.38 (s, 1H, CONH). ^{13}C -NMR (CDCl_3 -125 MHz) δ (ppm): 20.93 (CH_3), 24.53, 25.45, 50.27, 116.17, 118.63, 119.54, 119.64, 124.14, 129.74, 131.28, 133.86, 135.32, 135.44, 138.19, 148.46, 149.88, 152.32, 156.40, 158.06. MS (EI): m/z (%) 371 (M^++2 , 2), 370 (M^++1 , 12), 369 (M^+ , 43), 368 (M^+-1 , 4), 291 (62), 263 (100), 236 (23), 207 (10), 194 (2), 180 (7), 153 (3), 127 (2), 117 (5), 106 (14), 91 (9), 80 (35). Anal. Calcd. for $\text{C}_{22}\text{H}_{19}\text{N}_5\text{O}$ (369.42): C, 71.53; H, 5.18; N, 18.96. Found: C, 71.80; H, 4.83; N, 18.55.

4.1.1.9. (EZ)-N-(4-Chlorophenyl)-7-cyano-6-((pyridin-3-ylmethylene)amino)-2,3-dihydro-1H-pyrrolizine-5-carboxamide (11c)

Compound **8c** was refluxed with pyridine-3-carbaldehyde to afford compound **11c** as yellow crystalline product, m.p. 278-80 °C, yield 76%. $\text{IR}_{\text{vmax}}/\text{cm}^{-1}$ 3230, 3174 (NHs), 3053 (Ar C-H), 2213 (CN), 1660 (C=O). ^1H -NMR (CDCl_3 -400 MHz) δ (ppm): 2.59 (m, 2H, pyrrolizine CH_2 -2), 3.08 (t, 2H, $J = 7.6$ Hz, pyrrolizine CH_2 -1), 4.55 (t, 2H, $J = 7.2$ Hz, pyrrolizine CH_2 -3), 7.33 (d, 2H, $J = 8.7$ Hz, phenyl CH-3'+CH-5'), 7.49 (dd, 1H, $J = 7.9, 4.9$ Hz, pyridinyl CH-5''), 7.59 (d, 2H, $J = 8.7$ Hz, phenyl CH-2'+CH-6'), 8.18 (d, 1H, $J = 8.1$ Hz, pyridinyl CH-4''), 8.79 (d, 1H, $J = 4.3$ Hz, pyridinyl CH-6''), 9.16 (s, 1H, pyridinyl CH-2''), 9.23 (s, 1H,

methylene amino (N=CH)), 10.49 (s, 1H, CONH). ^{13}C -NMR (CDCl_3 -100 MHz) δ (ppm): 24.58, 25.45, 50.27, 115.98, 118.21, 120.82, 124.05, 129.08, 129.24, 131.05, 135.20, 136.64, 138.61, 148.06, 148.65, 150.05, 152.83, 157.05, 158.06. MS (EI): m/z (%) 392 (M^+ +3, 2), 391 (M^+ +2, 10), 390 (M^+ +1, 7), 389 (M^+ , 28), 388 (M^+ -1, 2), 311 (33), 263 (100), 236 (18), 207 (9), 194 (6), 180 (9), 153 (4), 127 (4), 117 (5), 106 (8), 91 (6), 80 (21). Anal. Calcd. for $\text{C}_{21}\text{H}_{16}\text{ClN}_5\text{O}$ (389.84): C, 64.70; H, 4.14; N, 17.96. Found: C, 65.10; H, 4.18; N, 18.08.

4.1.1.10. (EZ)-7-Cyano-6-((naphthalen-2-ylmethylene)amino)-N-phenyl-2,3-dihydro-1H-pyrrolizine-5-carboxamide (12a)

Compound **8a** was refluxed with 2-naphthaldehyde to afford compound **12a** as yellow crystals, m.p. 245-8°C, yield 79%. $\text{IR}_{\text{vmax}}/\text{cm}^{-1}$ 3281, 3181 (NHs), 3063 (Ar C-H), 2207 (CN), 1670 (C=O). ^1H -NMR (CDCl_3 -400 MHz) δ (ppm): 2.57 (m, 2H, pyrrolizine CH_2 -2), 3.06 (t, 2H, $J = 7.6$ Hz, pyrrolizine CH_2 -1), 4.56 (t, 2H, $J = 7.2$ Hz, pyrrolizine CH_2 -3), 7.09 (t, 1H, $J = 7.4$ Hz, aromatic proton), 7.31 (t, 2H, $J = 7.8$ Hz, phenyl CH-3'+CH5'), 7.62 (m, 5H, aromatic protons), 7.95 (d, 1H, $J = 8.1$ Hz, naphthalenyl proton), 8.04 (d, 1H, $J = 8.2$ Hz, naphthalenyl proton), 8.24 (d, 1H, $J = 7.2$ Hz, naphthalenyl proton), 8.67 (d, 1H, $J = 8.4$ Hz, naphthalenyl proton), 9.94 (s, H, methylene amino (N=CH)), 10.71 (s, H, CONH). ^{13}C -NMR (CDCl_3 -100 MHz) δ (ppm): 24.59, 25.46, 50.18, 116.52, 117.98, 119.69, 119.78, 123.17, 123.86, 125.31, 126.56, 127.95, 128.17, 129.01, 129.06, 130.99, 131.72, 133.03, 133.99, 138.34, 140.11, 148.26, 158.35, 158.50. MS (EI): m/z (%) 407 (M^+ +3, 1), 406 (M^+ +2, 5), 405 (M^+ +1, 31), 404 (M^+ , 100), 403 (M^+ -1, 5), 375 (3), 312 (99), 283 (43), 277 (38), 256 (19), 243 (6), 229 (12), 202 (14), 184 (13), 174 (14), 159 (14), 146 (4), 139 (16), 127 (38), 92 (12), 80 (53). Anal. Calcd. for $\text{C}_{26}\text{H}_{20}\text{N}_4\text{O}$ (404.46): C, 77.21; H, 4.98; N, 13.85. Found: C, 76.83; H, 5.21; N, 13.80.

4.1.1.11. (EZ)-7-Cyano-6-((naphthalen-2-ylmethylene)amino)-N-(4-tolyl)-2,3-dihydro-1H-pyrrolizine-5-carboxamide (12b)

Compound **8b** was refluxed with 2-naphthaldehyde to afford compound **12b** as yellow crystals, m.p. 262-5°C, yield 83%. $\text{IR}_{\text{vmax}}/\text{cm}^{-1}$ 3277, 3179 (NHs), 3059 (Ar C-H), 2211 (CN), 1660 (C=O), 1605, 1546 (C=C). ^1H -NMR (CDCl_3 -500 MHz) δ (ppm): 2.35 (s, 3H, CH_3), 2.61 (m, 2H, pyrrolizine CH_2 -2), 3.12 (t, 2H, $J = 7.3$ Hz, pyrrolizine CH_2 -1), 4.60 (t, 2H, $J = 7.0$ Hz, pyrrolizine CH_2 -3), 7.15 (d, 2H, $J = 7.7$ Hz, phenyl CH-3'+CH-5'), 7.52 (d, 2H, $J = 7.4$ Hz, phenyl CH-2'+CH-6'), 7.65 (m, 3H, naphthalenyl $\text{CH-1''+CH-7''+CH-8''}$), 7.99 (d, 1H, $J = 8.0$ Hz, naphthalenyl CH-9''), 8.08 (d, 1H, $J = 8.1$ Hz, naphthalenyl CH-6''), 8.27 (d, 1H, $J = 7.2$

Hz, naphthalenyl CH-4"), 8.74 (d, 1H, $J = 8.4$ Hz, naphthalenyl CH-3"), 9.97 (s, H, methylene amino (N=CH)), 10.67 (s, H, CONH). ^{13}C -NMR (CDCl_3 -100 MHz) δ (ppm): 20.88 (CH_3), 24.62, 25.51, 50.17, 116.57, 118.11, 119.70, 120.26, 123.25, 125.31, 126.58, 128.09, 128.19, 129.06, 129.51, 131.06, 131.73, 132.99, 133.47, 134.01, 135.76, 139.99, 148.14, 158.38, 158.43. MS (EI): m/z (%) 421 ($\text{M}^+ + 3$, 1), 420 ($\text{M}^+ + 2$, 4), 419 ($\text{M}^+ + 1$, 26), 418 (M^+ , 83), 417 ($\text{M}^+ - 1$, 4), 325 (2), 312 (100), 291 (34), 283 (27), 256 (14), 244 (6), 229 (10), 209 (11), 184 (12), 174 (5), 155 (29), 146 (3), 127 (27), 92 (2), 80 (21). Anal. Calcd. for $\text{C}_{27}\text{H}_{22}\text{N}_4\text{O}$ (418.49): C, 77.49; H, 5.30; N, 13.39. Found: C, 77.05; H, 5.61; N, 13.28.

4.1.1.12. (EZ)-N-(4-Chlorophenyl)-7-cyano-6-((naphthalen-2-ylmethylene)amino)-2,3-dihydro-1H-pyrrolizine-5-carboxamide (12c)

Compound **8c** was refluxed with 2-naphthaldehyde to afford compound **12c** as yellow crystals, m.p. 276-8 °C, yield 77%. $\text{IR}_{\text{vmax}}/\text{cm}^{-1}$ 3421, 3173 (NHs), 3050 (Ar C-H), 2214 (CN), 1669 (C=O). ^1H -NMR (CDCl_3 -500 MHz) δ (ppm): 2.62 (m, 2H, pyrrolizine CH_2 -2), 3.12 (t, 2H, $J = 7.4$ Hz, pyrrolizine CH_2 -1), 4.58 (t, 2H, $J = 7.1$ Hz, pyrrolizine CH_2 -3), 7.28 (d, phenyl CH-3'+CH-5'), 7.56 (d, 2H, $J = 7.6$ Hz, phenyl CH-2'+CH-6'), 7.65 (m, 3H, naphthalenyl CH-1''+CH-7''+CH-8''), 8.0 (d, 1H, $J = 7.9$ Hz, naphthalenyl CH-9''), 8.09 (d, 1H, $J = 8.1$ Hz, naphthalenyl CH-6''), 8.22 (d, 1H, $J = 7.2$ Hz, naphthalenyl CH-4''), 8.74 (d, 1H, $J = 8.2$ Hz, naphthalenyl CH-3''), 9.95 (s, H, methylene amino (N=CH)), 10.77 (s, H, CONH). ^{13}C -NMR (CDCl_3 -100 MHz) δ (ppm): 24.63, 25.47, 50.17, 116.38, 117.72, 120.81, 120.93, 123.27, 125.28, 126.65, 128.27, 128.39, 128.66, 128.97, 129.14, 131.00, 131.62, 133.17, 134.04, 136.95, 140.24, 148.43, 158.48, 158.82. MS (EI): m/z (%) 442 ($\text{M}^+ + 4$, 1), 441 ($\text{M}^+ + 3$, 7), 440 ($\text{M}^+ + 2$, 23), 439 ($\text{M}^+ + 1$, 22), 438 (M^+ , 68), 437 ($\text{M}^+ - 1$, 5), 409 (1), 328 (8), 312 (99), 283 (30), 256 (17), 243 (5), 229 (10), 202 (7), 184 (10), 174 (16), 155 (42), 146 (6), 139 (14), 127 (59), 92 (8), 80 (56), 64 (100). Anal. Calcd. for $\text{C}_{26}\text{H}_{19}\text{ClN}_4\text{O}$ (438.91): C, 71.15; H, 4.36; N, 12.77. Found: C, 70.91; H, 4.57; N, 12.69.

4.2. Pharmacological screening

4.2.1. Growth inhibition

4.2.1.1. Cell cultures

Human breast cancer (MCF-7), human non-small cell lung cancer (A549) and human hepatoma (Hep3B) cell lines were obtained from the American Type Culture Collection (Manassas, VA). All cells were cultured in Dulbecco's modified Eagles medium / F12 medium (DMEM/F-12,

Gibco, Grand Island, NY) or DMEM supplemented with 10% fetal bovine serum (FBS; Gibco) in a humidified incubator containing 5% CO₂ at 37° C.

4.2.1.2. Cell viability analysis

The 3-(4,5-dimethylthiazol-2-yl)-2,5-diphenyl-2H-tetrazolium bromide (MTT) assay was used to measure the effect of the new compounds on the cell viability of cancer cells as previously reported [29]. Cells were seeded for 24 h in 96-well flat-bottomed plates. The seeded cells were then treated with the test compounds in 5% FBS-supplemented DMEM/F-12 or DMEM for the indicated time intervals. DMSO vehicle at the same concentration used in drug-treated cells was used for the controls. After the treatment, cancer cells were incubated in the same medium containing 0.5 mg/mL MTT for 3 h at 37 °C. The reduced MTT was dissolved in DMSO (200 µL) and microplate reader was used to determine the absorbance at 570 nm. The results were represented in **Table 1**.

4.2.2. *In vitro* COX-1/2 inhibitory assay

All the new compounds **9-12** were tested for their inhibitory activity against both COX-1 (ovine) and COX-2 (human recombinant) enzymes. COX inhibitor screening assay kit (Item No. 560131) provided from Cayman Chemicals, Ann Arbor, MI, USA, was used. The assay was done following the manufacturer's instructions and as mentioned before [33]. The results were presented as IC₅₀ (µM) and compared with that of indomethacin and celecoxib as reference drugs, **Table 2**.

4.2.3. Kinase profiling assay

The kinases inhibition assay was done by KINEXUS Corporation, Vancouver, BC, Canada. Using the radiolabeled ATP determination method. Compound **12b** was selected to evaluate its inhibitory activity against 20 kinases. The assay was performed according to the previous report [34]. Imatinib was used as reference drug and blank control was set up and the corrected activity for protein kinase target was determined. The results were presented as % inhibition, **Table 3**.

4.2.4. Caspase activation assay

Caspase-Glo 3/7 luminescence assay kit (Promega, Madison, WI) was used to determine caspase 3/7 and caspase-8 activities in lung carcinoma A549 cells treated with the tested compounds. The assay kit was used according to the manufacturer's instructions and as mentioned before

[37]. Cells were plated at 1×10^4 (100 mL/well) into clear bottom, opaque wall 96-well tissue culture plates. Cells were incubated for 24 h. cells were treated with compounds **9a**, and **12a-c** for 24 h after removal of the medium. The activity of caspase 3/7 were assessed according to manufacturer's instructions. Luminometer was used to determine the luminescence of the plates and results were represented in **Fig. 3**.

4.2.5. Determination of cell cycle perturbations

Cell cycle distribution analysis was performed based on the previously described method [38]. Propidium iodide (PI) fluorescence-labelled cell nuclei were suspended in a stream of fluid, and an argon laser $A^{488/645}$ was used to excite PI (emission A^{617}), and emissions above A^{550} were collected. MCF-7 cells were seeded in 6-well plates at 1×10^5 cells/well in 2 mL medium, and were left to attach overnight, before treatment with control or compound **12b** ($n = 2$) to final concentrations: 0, 1, 5 and 10 μM . Then, plates were incubated for 24 h. After incubation, medium was collected and kept on ice. Cells were washed with ice-cold phosphate-buffered saline (PBS, 2 \times). Trypsin (0.5 mL) was added to each well and incubated at 37 $^\circ\text{C}$ for 5 min, detached cells were pooled with the floating cell suspension. Then tubes were centrifuged at 1200 rpm for 5 min at 4 $^\circ\text{C}$ and the supernatant was discarded. Pellets were washed in 1 mL of PBS, centrifuged and fixed overnight in 70% ice cold ethanol. Then pellets were centrifuged, re-suspended in PBS with the addition of ribonuclease A (15 min), followed by PI (2 $\mu\text{L}/\text{mL}$). Samples were held on ice, and analysed by flow cytometry (Beckman counter, FC500). Data analysis of DNA contents (PI bound to DNA) of 20000 events was carried out using Expo 32 software. Doublets were differentiated from single cells in the G_2/M phase by gating them out manually. The results were presented in **Fig. 4**.

4.2.6. Annexin V PI/FITC apoptosis assay

Apoptosis was quantified by detecting cell surface exposure of phosphatidylserine (PS) in apoptotic cells using Annexin V Fluorescein Isothiocyanate/Propidium Iodide (FITC/PI) [39]. MCF-7 cells were seeded in 6 well plates at 1×10^5 cells/well in 2 mL medium. They were left to attach overnight at 37 $^\circ\text{C}$, before treatment with compound **12b** for 24 h incubation periods at final concentrations of 0, 1, 5, 10, 100 μM . Cells were inspected microscopically before and after treatment to observe morphological changes. Floating cells were collected in tubes and kept on ice, while remaining cells were detached with trypsin, incubated at 37 $^\circ\text{C}$ for 3 min, and pooled. Cells were centrifuged at 1,200 rpm for 5 min at 4 $^\circ\text{C}$. Supernatants were discarded and 2 mL fresh medium added to each tube, and kept on ice. Cells (1×10^5) were transferred to 12x75

mm tubes. Cell solutions were washed (1 mL PBS) and centrifuged again. Supernatants were discarded and pellets re-suspended in 100 μ L \times 1 binding buffer (10 mM 4-(2-hydroxyethyl)-1-piperazineethanesulfonic acid (HEPES), 0.14 M NaCl, 2.5 mM CaCl₂, pH 7.4, diluted in dH₂O 1:10, stored at 4 °C), and shaken gently. Annexin V FITC (10 μ L, stored at 4 °C) was added to each sample and incubated at room temperature in dark for 15 min. A further 400 μ L 1x binding buffer and 10 μ L PI (0.05 mg/mL in PBS) were added. Tubes were shaken gently and left to set for 10 min in the dark on ice. Samples were analyzed by flow cytometry within 1 h. Viable cells were differentiated from early and late apoptotic/necrotic cells by Annexin V (x axis) and PI staining (y axis). The results were presented in **Fig. 5**.

4.2.7. Molecular docking study

4.2.7.1. Comparative GOLD Molecular Docking study into COX-1 and COX-2

A comparative docking study for compounds **9-12** were performed into COX-1 and COX-2 enzymes. The crystal structure of ovine COX-1 (PDB: 1eqg) [40] complexed with ibuprofen (2-(4-isobutylphenyl)propionic acid; IBP) and the crystal structure of human COX-2 (PDB: 5kir) [41] in complex with its bound ligand Rofecoxib (Vioxx) were retrieved from the Protein Data Bank, <http://www.rcsb.org/pdb/home/home.do>. The key amino acids of the active site were identified using data in PDB sum, <http://www.ebi.ac.uk/pdbsum/>.

The constructed 3D structures of our twelve designed compounds (**9a-c**, **10a-c**, **11a-c**, and **12a-c**) were energetically minimized by using MOPAC with 100 iterations and minimum RMS gradient of 0.10. GOLD software package version 5.2.2 (Cambridge Crystallographic Data Centre, Cambridge, U.K.) was used in this study [49]. The Hermes visualizer in the GOLD Suite and Accelrys Discovery studio were utilized for preparation of the receptor and ligands for flexible docking. The docking was done within 15 Å diameters from the reference co-crystallized ligands (IBP and RCX). The binding site of COX-1 is composed of the following amino acids: Leu115, Val116, Val119, Arg120, Val349, Tyr355, Asn382, Tyr385, His386, His388, Met522, and Ala527. The binding site was defined by including all residues within the flood fill radius 5 Å of the origin: -26.685, 33.900, and 200.400 Å of the co-crystallized IBP ligand coordinates. The selected flexible residues were: Arg120, and Tyr355.

The binding site of COX-2 is composed of the following amino acids: His90, Arg120, Gln192, Tyr348, Val349, His351, Leu352, Ser353, Tyr355, Leu359, Tyr385, Trp387, Arg513, Ala516, Phe518, Met522, Val523, Glu524, Ser530, and Leu531. The binding site was defined by including all residues within the flood fill radius 5 Å of the origin: 23.339, 1.256, and 34.701 Å

of the co-crystallized IBP ligand coordinates. The selected flexible residues were: His90, Arg513, and Ala527. Gold flexible ligand docking generated 10 poses of each ligand, which were ranked using the Gold-score scoring function. The top-ranked pose with highest Gold-Score fitness was analyzed using Accelrys Discovery Studio to reveal the hydrogen bond interaction and binding mode within the binding domain. The docking parameters were adjusted to default values during the pose selection and enrichment studies. We used 10 genetic algorithms (GA) docking runs with internal energy offset. For pose reproduction analysis, the radius of the binding pocket was set as the maximal atomic distance from the geometrical center of the ligand plus 3Å. The top-ranked docking pose was retained for the 3D cumulative success rate analysis. The Genetic Algorithm default settings were accepted as population size 100, selection pressure 1.1, number of operations 50,000, number of islands 5, niche size 2, migrate 10, mutate 95, and crossover 95. All other parameters accepted the default settings. The results of the docking study of compound **9-12** into COX-1 and COX-2 were presented in **Table 4** and **Fig. 7**.

4.2.7.2. AutoDock Molecular Docking into different kinases

A docking study of **12b** into ALK1 and Aurora A. AutoDock 4.2 was used in the docking studies and Discovery Studio Visualizer (v16.1.0.15350) was used in visualization of the docking poses. The binding modes and binding free energies of the new pyrrolizines were determined and compared with those of the native ligands

The crystal structure of ALK1 (pdb code: 3MY0) [47] and Aurora A (pdb code: 2W1C) [48] were obtained from protein data bank (<http://www.rcsb.org/pdb>). The protein structure was prepared by delating water molecules and the native ligands. Validation of the docking studies were done by re-docking the native ligands with their corresponding kinases. The binding modes and interactions of the native ligands with the key amino acids in the active site were identified and compared with the reported data. The re-docked native ligands superimposed onto the position of the

4.2.7.2.1. Preparation of the protein kinases pdbqt files

The crystal structures of the proteins co-crystallized with the native ligands were obtained from Protein Data Bank (<http://www.rcsb.org/pdb>) as pdb files. ALK1 (pdb code: 3MY0) was obtained in X-ray resolution of 2.65 Å and Aurora A (pdb code: 2W1C) in X-ray resolution of 3.24 Å [47-48]. The discovery studio visualizer (DSV, v16.1.0.15350) was used to handle the protein structures. During the preparation of the proteins, water molecules and bound ligands were removed to avoid interference with the study. The docking study was performed using

AutoDock 4.2, AutoDock tools (ADT) 1.5.6 was used in preparation and analysis of the docking results. The pdb format of the test compounds **9-12a-c** were prepared using Chem3D Ultra 8.0 followed by MOPAC energy minimization.

4.2.7.2.2. Preparation of the ligands 9-12a-c

The chemical structures of the ligands were sketched using ChemDraw Ultra 8.0 software. Chem3D Ultra 8.0 was used in the preparation of the ligand in the pdb format. The energies of the ligands were minimized using MOPAC with 100 iterations. The AutoDock Tool 1.5.6 was used to read the pdb files of the ligands, add the hydrogens, compute Gasteiger charges, and to convert the pdb into the pdbqt format for docking study. The docking scenarios was done using flexible ligands where the rotatable bonds in the ligands were assigned using AutoDock tools (ADT) 1.5.6.

4.2.7.2.3. Preparation of affinity maps and running AutoGrid

Preparation of the Grid parameter files by AutoDock was done using AutoGrid which generate a map for each type of atom in the docking area. The 3D grid with final size of 60 x 60 x 60 Å with 0.375 Å spacing was used. The center of the grid was assigned for ALK1 at 60.442, -52.275, and -29.296 Å, for Aurora A at 3.177, 33.363, and 4.130 Å.

4.2.7.2.4. Preparation of docking parameter file and running AutoDock

The protein molecule and the ligand were selected to run AutoDock and perform the docking calculations. Docking parameter file was set to the default values. In this study, we have set the protein as a rigid file while ligands were used as flexible molecules. Lamarckian Genetic Algorithm was set as the search parameter. After running AutoDock, the top ten conformations of the protein-ligand complex were clustered. The docking poses were scored and ranked in decreasing order of their binding free energy.

4.2.7.2.5. Analysis and visualization of the results

AutoDock 4.2. was used in the analysis of the docking results, determination of the binding free energy (ΔG_b), and inhibition constants (K_i). Binding mode of the ligand and type of ligand-protein interactions were vitalized using discovery studio visualizer (v16.1.0.15350). The 2D/3D binding mode was visualized showing both hydrogen bonding and hydrophobic interactions. The results were presented in **Table 5** and **Fig. 8**.

Acknowledgement

The authors would like to thank the Deanship of Scientific Research at Umm Al-Qura University for the continuous support. This work was supported financially by the Deanship of Scientific Research at Umm Al-Qura University, Makkah, Kingdom of Saudi Arabia to Dr. Ahmed Mahmoud Gouda Said (Grant Code: **15-MED-3-1-0059**).

Supplementary data

Supplementary data including all spectral data and copies of IR, Mass, $^1\text{H-NMR}$ and $^{13}\text{C-NMR}$ spectra, of all final compounds was provided with this manuscript (**Fig. S1-S36**).

Conflict of Interest

All authors of this manuscript have not declared any conflict of interest.

References

1. Wallerand, H.; Reiter, R. R.; Ravaud, A. *Curr. Opin. Urol.* **2008**, *18*, 524–532.
2. Siegel, R.; Miller, K.; Jemal, A. *CA Cancer J. Clin.* **2015**, *65*, 5-29.
3. Bonezzi, K.; Taraboletti, G.; Borsotti, P.; Bellina, F.; Rossi, R.; Giavazzi, R. *J. Med. Chem.* **2009**, *52*, 7906–7910.
4. Kobayashi, S.; Boggon, T. J.; Dayaram, T.; Janne, P. A.; Kocher, O.; Meyerson, M.; Johnson, B. E.; Eck, M. J.; Tenen, D. G.; Halmos, B. *N. Engl. J. Med.* **2005**, *352*, 786–792.
5. Thomas, H.; Coley, H. M. *Cancer Control* **2003**, *10*, 159–165.
6. Xie, L.; Bourne, P. E. *Front. Pharmacol.* **2015**, *6*, 1–5.
7. Rao, C. V.; Janakiram, N. B.; Madka, V.; Devarkonda, V.; Brewer, M.; Biddick, L.; Lightfoot, S.; Steele, V. E.; Mohammed, A. *Oncotarget* **2015**, *6*, 33290–305.
8. Mohammed, A.; Janakiram, N. B.; Pant, S.; Rao, C. V. *Cancers (Basel)*. **2015**, *7*, 1499–1542.
9. Kumar, G.; Patlolla, J. M. R.; Madka, V.; Mohammed, A.; Li, Q.; Zhang, Y.; Biddick, L.; Singh, A.; Gillaspay, A.; Lightfoot, S.; Steele, V. E.; Kopelovich, L.; Rao, C. V. *Am. J. Cancer Res.* **2016**, *6*, 894–909.

10. Tauler, J.; Mulshine, J. L. *PPAR Res.* **2008**, *2008*, 750238.
11. Mohammed, A.; Janakiram, N. B.; Brewer, M.; Vedala, K.; Steele, V. E.; Rao, C. V. *Neoplasia* **2013**, *15*, 481–90.
12. Miles, D.; von Minckwitz, G.; Seidman, A. D. *Oncologist* **2002**, *7 Suppl 6*, 13–19.
13. Maione, P.; Gridelli, C.; Troiani, T.; Ciardiello, F. *Oncologist* **2006**, *11*, 274–284.
14. Broxterman, H. J.; Georgopapadakou, N. H. *Drug Resist. Updat.* **2005**, *8*, 183–197.
15. Narayanan, N. K.; Nargi, D.; Attur, M.; Abramson, S. B.; Narayanan, B. A. *Anticancer Res.* **2007**, *27*, 2393–2402.
16. Liu, W.; Zhou, J.; Bensdorf, K.; Zhang, H.; Liu, H.; Wang, Y.; Qian, H.; Zhang, Y.; Wellner, A.; Rubner, G.; Huang, W.; Guo, C.; Gust, R. *Eur. J. Med. Chem.* **2011**, *46*, 907–913.
17. Kus, G.; Oztoccu-Vatan, P.; Uyar, R.; Kabadere, S. *Acta Biol. Hung.* **2013**, *64*, 438–52.
18. Tavolari, S.; Bonafè, M.; Marini, M.; Ferreri, C.; Bartolini, G.; Brighenti, E.; Manara, S.; Tomasi, V.; Laufer, S.; Guarnieri, T. *Carcinogenesis* **2008**, *29*, 371–380.
19. Tavolari, S.; Munarini, A.; Storci, G.; Laufer, S.; Chieco, P.; Guarnieri, T. *Cancer Lett.* **2012**, *321*, 187–194.
20. Lisowski, V.; Enguehard, C.; Lancelot, J.; Caignard, D.; Lambel, S.; Leonce, S.; Pierre, A.; Atassi, G.; Renard, P.; Rault, S. *Bioorg. Med. Chem. Lett.* **2001**, *11*, 2205–2208.
21. Rochais, C.; Cresteil, T.; Perri, V.; Jouanne, M.; Lesnard, A.; Rault, S.; Dallemagne, P. *Cancer Lett.* **2013**, *331*, 92–98.
22. Lisowski, V.; Leonce, S.; Kraus-Berthier, L.; Sopkova-de Oliveira Santos, J.; Pierre, A.; Atassi, G.; Caignard, D.-H.; Renard, P.; Rault, S. *J. Med. Chem.* **2004**, *47*, 1448–1464.
23. Gouda, A. M.; Abdelazeem, A. H.; Arafa, E.-S. A.; Abdellatif, K. R. A. *Bioorg. Chem.* **2014**, *53*, 1–7.
24. Gouda, A. M.; Abdelazeem, A. H. *Eur. J. Med. Chem.* **2016**, *114*, 257–292.
25. Belal, A.; El-Gendy, B. E.-D. M. *Bioorg. Med. Chem.* **2014**, *22*, 46–53.
26. Etienne, A.; Y. Correia, Y. *Bull. Soc. Chem.*, **1969**, *10*, 3704–3712.
27. Jacobs, W. A.; Heidelberger, M. *J. Am. Chem. Soc.* **1917**, *39*, 1435–1439.
28. Gouda, A.; Ali, H.; Almalki, W.; Azim, M.; Abourehab, M.; Abdelazeem, A. *Molecules* **2016**, *21*, 201.
29. Arafa, E. A.; Abdelazeem, A. H.; Arab, H. H.; Omar, H. A. *Acta Pharmacol. Sin.* **2014**, *35*, 394–400.
30. Sarkar, F. H.; Adsule, S.; Li, Y.; Padhye, S. *Mini Rev. Med. Chem.* **2007**, *7*, 599–608.
31. Ramon, S.; Woeller, C. F.; Phipps, R. P. *Curr. Angiogenes.* **2013**, *2*, 135–142.

32. Chien, C.-C.; Ko, C.-H.; Shen, S.-C.; Yang, L.-Y.; Chen, Y.-C. *J. Cell. Physiol.* **2012**, *227*, 3128–3137.
33. Handler, N.; Jaeger, W.; Puschacher, H.; Leisser, K.; Erker, T. *Chem. Pharm. Bull. (Tokyo)*. **2007**, *55*, 64–71.
34. Elsayed, M. S. A.; El-Araby, M. E.; Serya, R. A. T.; El-Khatib, A. H.; Linscheid, M. W.; Abouzid, K. A. M. *Eur. J. Med. Chem.* **2013**, *61*, 122–131.
35. Wolf, B. B.; Schuler, M.; Echeverri, F.; Green, D. R. *J. Biol. Chem.* **1999**, *274*, 30651–30656.
36. Lamkanfi, M.; Kanneganti, T.-D. *Int. J. Biochem. Cell Biol.* **2010**, *42*, 21–24.
37. Omar, H. A.; Arafa, E.-S. A.; Maghrabi, I. A.; Weng, J.-R. *Basic Clin. Pharmacol. Toxicol.* **2014**, *114*, 464–471.
38. Nicoletti, I.; Migliorati, G.; Pagliacci, M. C.; Grignani, F.; Riccardi, C. *J. Immunol. Methods* **1991**, *139*, 271–279.
39. Vermes, I.; Haanen, C.; Steffens-Nakken, H.; Reutelingsperger, C. *J. Immunol. Methods* **1995**, *184*, 39–51.
40. Selinsky, B. S.; Gupta, K.; Sharkey, C. T.; Loll, P. J. *Biochemistry* **2001**, *40*, 5172–5180.
41. Orlando, B. J.; Malkowski, M. G. *Acta Crystallogr. Sect. F, Struct. Biol. Commun.* **2016**, *72*, 772–776.
42. Giamas, G.; Stebbing, J.; Vorgias, C. E.; Knippschild, U. *Pharmacogenomics* **2007**, *8*, 1005–1016.
43. Cunha, S. I.; Pietras, K. *Blood* **2011**, *117*, 6999–7006.
44. D’Assoro, A. B.; Haddad, T.; Galanis, E. *Front. Oncol.* **2015**, 295.
45. Deshpande, A.; Sicinski, P.; Hinds, P. W. *Oncogene* **2005**, *24*, 2909–2915.
46. Guo, X.; Williams, J. G.; Schug, T. T.; Li, X. *J. Biol. Chem.* **2010**, *285*, 13223–13232.
47. Kerr, G.; Sheldon, H.; Chaikuad, A.; Alfano, I.; von Delft, F.; Bullock, A. N.; Harris, A. L. *Angiogenesis* **2015**, *18*, 209–217.
48. Howard, S.; Berdini, V.; Boulstridge, J. A.; Carr, M. G.; Cross, D. M.; Curry, J.; Devine, L. A.; Early, T. R.; Fazal, L.; Gill, A. L.; Heathcote, M.; Maman, S.; Matthews, J. E.; McMenamin, R. L.; Navarro, E. F.; O’Brien, M. A.; O’Reilly, M.; Rees, D. C.; Reule, M.; Tisi, D.; Williams, G.; Vinković, M.; Wyatt, P. G. *J. Med. Chem.* **2009**, *52*, 379–388.
49. Verdonk, M. L.; Cole, J. C.; Hartshorn, M. J.; Murray, C. W.; Taylor, R. D. *Proteins* **2003**, *52*, 609–623.

Figures, schemes and table captions

Fig. 1. Pyrrolizine-based anticancer agents with their IC₅₀ values against different cancer cells

Fig. 2. Rational design of scaffold A

Scheme 1. Reagents and reaction conditions: (a) (CH₃)₂SO₄, benzene, CH₂(CN)₂; (b) ClCH₂COCl, AcOH, CH₃COONa; (c) K₂CO₃, acetone, reflux, 24 h.

Scheme 2. Reagent and reaction conditions: (a) pyridine-3-carbaldehyde, AcOH, EtOH, reflux, 4 h; (b) furan-2-carbaldehyde, AcOH, EtOH, reflux, 4 h; (c) thiophene-2-carbaldehyde, AcOH, EtOH, reflux, 4 h; (d) 2-naphthaldehyde, AcOH, EtOH, reflux, 4 h.

Table 1. IC₅₀ values of compounds **9-12** against MCF-7, A549 and Hep3B cancer cell lines

Cells were treated with the new compound or vehicle for 48 h. and the results were presented as mean ± S.D. (n = 6)

Table 2: *In vitro* COX-1/2 enzymes inhibition results of compound **9-12**.

^a IC₅₀ was calculated using three determinations for COX-1 (ovine) and COX-2 (human recombinant) screening assay kit (Cat. No 560131, Cayman Chemicals Inc., Ann Arbor, MI, USA); ^b *in vitro* COX-2 selectivity index (*SI*) = IC₅₀ of COX-1/ IC₅₀ of COX-2.

Table 3: The activation and inhibition of compound **12b** and imatinib against 20 different kinases at 10 μM concentration.

Negative values indicate inhibition and positive value indicate activation

Fig. 3. Caspase-Glo 3/7 assay of lung carcinoma A549 cells treated with compounds **9a** (■), **12a** (▣), **12b** (▢), and **12c** (▤), controls received equivalent amount of DMSO (vehicle). Columns, mean; bars, S.D. (n = 5). * p < 0.05, ** p < 0.01 as compared to vehicle (DMSO)-treated cells using one-way ANOVA followed by Dunnett's multiple comparison test.

Fig. 4. Cell cycle phases of MCF-7 treated with compound **12b** for 24h (concentration, x axis); cell count (percent, y axis). Controls received equivalent amount of DMSO (vehicle). Columns, mean; bars, S.D. (n = 3). * p < 0.05, ** p < 0.01 as compared to vehicle (DMSO)-treated cells using one-way ANOVA followed by Dunnett's multiple comparison test

Fig. 5. Annexin V phases of MCF-7 cancer cells treated for 24 h with DMSO control (a), compound **12b** at 1 μM (b), 5 μM (c), 10 μM (d); Data shown in the mean % ± SD (n = 3). Experiment was repeated 3x.

Fig. 6. a) Validation of the GOLD program by docking of ibuprofen into COX-1 (PDB: 1eqg); **b)** Validation of the GOLD program by docking of rofecoxib (Vioxx) into COX 2 (PDB: 5kir). The docked ligands (ball and stick) were identically superimposed on the co-crystallized IBP and RCX ligands (yellow sticks) within RMSD of 0.64 and 0.81 Å, respectively revealing a successful docking protocol.

Table 4. The docking results for the top five ranks of the compounds docked into COX-1 (1EQG) [40] and COX-2 (5KIR) [41] in comparison to the native bound inhibitors involving GOLD5.2.2

Fig. 7. a): Comparative docking mode of compound **12b** (yellow ball and stick) into COX1 (PDB: 1eqg), it exhibited a Goldscore fitness of 35.92, RMSD of 2.66Å, and one hydrogen bond with Arg120; **b)** docking mode of compound **12b** into COX 2 (PDB: 5kir), it revealed a

Goldscore fitness of 88.15, RMSD of 0.58Å, and two hydrogen bond with Tyr355 and Phe518. (--) Hydrogen bond; (--) π -alkyl and π - π hydrophobic interaction; and (--) π -cation-electrostatic interaction.

Table 5. Results of the docking of compounds **12b** into ALK1 (pdb code: 3MY0) and Aurora A (pdb code: 2W1C) in comparison to the native ligands

^a Binding free energy; ^b Inhibition constant; ^c Hydrogen bonds; ^d length in angstrom (Å),

^e electrostatic attraction (ionic bond).

Fig. 8. **a)** 3D Docking mode of compound **12b** into ALK1 (pdb code: 3MY0); **b)** 2D Docking mode of compound **12b** into ALK1; **c)** 3D Docking mode of compound **12b** into Aurora A (pdb code: 2W1C); **d)** 2D Docking mode of compound **12b** into Aurora A. Hydrogen bonds were represented as (■ ■ ■), hydrophobic interactions including pi-sigma as (■ ■ ■), alkyl as (■ ■ ■) and pi-alkyl as (■ ■ ■) and unfavorable interaction as (■ ■ ■).

Highlights

- A novel series of twelve pyrrolizines (**9-12a-c**) were designed and synthesized
- The anticancer activity was evaluated against MCF-7, A549, and Hep3B cells using MTT assay
- Compound **12b** showed IC₅₀ value of 3.24 μ M against A549 cell line
- The new compounds inhibited COX-1 and COX-2 with the selectivity index of 8.38-113.1 range
- Compound **12b** revealed a weak to moderate inhibition of six different protein kinases
- Compounds **12a** and **12b** exhibited the highest activation of caspase-3/7 in A549 cells
- Cell cycle analysis and Annexin V PI/FITC assay revealed an accumulation of MCF-7 tumor cells in the S-phase and an apoptotic induction by compound **12b**.

ACCEPTED MANUSCRIPT